



HAL
open science

Analysis of the Transport of Aerosols over the North Tropical Atlantic Ocean Using Time Series of POLDER/PARASOL Satellite Data

Hélène Fréville, Malik Chami, Marc Mallet

► **To cite this version:**

Hélène Fréville, Malik Chami, Marc Mallet. Analysis of the Transport of Aerosols over the North Tropical Atlantic Ocean Using Time Series of POLDER/PARASOL Satellite Data. *Remote Sensing*, 2020, 12 (5), pp.757. 10.3390/rs12050757 . insu-02497649

HAL Id: insu-02497649

<https://insu.hal.science/insu-02497649>

Submitted on 3 Mar 2020

HAL is a multi-disciplinary open access archive for the deposit and dissemination of scientific research documents, whether they are published or not. The documents may come from teaching and research institutions in France or abroad, or from public or private research centers.

L'archive ouverte pluridisciplinaire **HAL**, est destinée au dépôt et à la diffusion de documents scientifiques de niveau recherche, publiés ou non, émanant des établissements d'enseignement et de recherche français ou étrangers, des laboratoires publics ou privés.

Article

Analysis of the Transport of Aerosols over the North Tropical Atlantic Ocean Using Time Series of POLDER/PARASOL Satellite Data

Hélène Fréville ^{1,*} , Malik Chami ^{2,3}  and Marc Mallet ¹

¹ Centre National de Recherches Météorologiques, Météo France/CNRS, UMR3589 Toulouse, France; marc.mallet@meteo.fr

² Laboratoire Atmosphères Milieux Observations Spatiales (LATMOS), CNRS-INSU, Sorbonne Université, 75005 Paris, France; malik.chami@upmc.fr

³ Institut Universitaire de France, Ministère de l'Éducation Nationale, de l'Enseignement Supérieur et de la Recherche, 1 rue Descartes, CEDEX 05, 75231 Paris, France

* Correspondence: helene.freville@meteo.fr

Received: 15 January 2020; Accepted: 14 February 2020; Published: 25 February 2020



Abstract: The time series of total, fine and coarse POLAC/PARASOL aerosol optical depth (AOD) satellite products (2005–2013) processed by the POLAC algorithm are examined to investigate the transport of aerosols over the North Tropical Atlantic Ocean, a region that is characterized by significant dust aerosols events. First, the comparison of satellite observations with ground-based measurements acquired by AERONET ground-based measurements shows a satisfactory consistency for both total AOD and coarse mode AOD (i.e., correlation coefficients of 0.75 and bias ranging from -0.03 to 0.03), thus confirming the robustness and performance of POLAC/PARASOL data to investigate the spatio-temporal variability of the aerosols over the study area. Regarding fine mode aerosol, POLAC/PARASOL data present a lower performance with correlation coefficient ranging from 0.37 to 0.73. Second, the analysis of POLAC/PARASOL aerosol climatology reveals a high contribution of the coarse mode of aerosols (AOD_c between 0.1 and 0.4) at long distance from the African sources, confirming previous studies related to dust transport. The POLAC/PARASOL data were also compared with aerosol data obtained over the North Tropical Atlantic Ocean from MACC and MERRA-2 reanalyses. It is observed that the total AOD is underestimated in both reanalysis with a negative bias reaching -0.2 . In summary, our results thus suggest that satellite POLAC/PARASOL observations of fine and coarse modes of aerosols could provide additional constraints useful to improve the quantification of the dust direct radiative forcing on a regional scale but also the biogeochemical processes such as nutrient supply to the surface waters.

Keywords: satellite remote sensing; atmospheric optics; aerosol transport

1. Introduction

Composed of fine solid particles or liquid droplets suspended in air, aerosols constitute an important part of the atmosphere. Through their microphysical and optical properties, they interact with solar and terrestrial radiation, alter cloud amount and radiative properties (e.g., [1–5]), fertilize ocean and land, and regulate carbon uptake (e.g., [6,7]) with ensuing impacts on climate (e.g., [8–10]). The sensitivity of radiative forcing to the variations of the aerosol optical properties defines the impact of aerosols on climate change and must be taken into account in climate scenarios (e.g., [11]). Yet, it is still difficult to obtain an accurate estimate of the radiative impact of aerosols. The scarcity of information on aerosol optical properties is one of the greatest uncertainties in the evaluation of climate forcing (e.g., [12–15]).

Anthropogenic aerosols mostly contribute to the fine mode mass fraction (effective radius below 1 μm) present in the atmosphere while natural aerosols mostly contribute to the coarse mode (effective radius above 1 μm). This is particularly the case for mineral dust particles which represent the main contributor to the total number of natural aerosols in the atmosphere (e.g., [9]). Desert dust also represent around 70% of global aerosol mass and 25% of the total aerosol optical depth (AOD) at visible wavelengths (e.g., [16,17]). Their primary source of emission is the Sahara desert of Northern Africa (e.g., [18]). Over North Africa, the harmattan winds, the Saharan heat low and the west african monsoon circulation are the three major atmospheric circulation regimes that contribute to make North Africa the most active dust source region on Earth (e.g., [19]). That is also where the Saharan air layer (SAL) originates, an elevated layer of extremely dry and dusty air having its base at 900–1800 m and its top below 5500 m (e.g., [20–22]). The SAL is responsible for the main dust transport over extensive areas from the Northern Africa to the Caribbean (e.g., [23,24]), the southern United States (e.g., [25]) and northeastern South America (e.g., [10,26]). It can be observed all year round, reaching its peak of intensity during summer months (e.g., [6,10,25,27–35]).

Satellite sensors are well-suited for monitoring aerosols on a global scale (e.g., [8,9,36]), especially when they are combined with ground-based measurements (e.g., [37–40]). In such a context, the development of inversion methods to derive aerosol optical properties from satellite data is in constant progress (e.g., [41–48]). Satellite passive remote sensing with polarization capabilities is one of the most promising and often underexploited approach for the detection of aerosol. The use of multispectral and multidirectional polarization measurements of scattered sunlight could improve the retrieval of different aerosol properties such as the aerosol optical thickness or their microphysical properties (size distribution, composition and shape) due to the sensitivity of the polarized radiation to the real part of the refractive index (e.g., [49]). Previous studies showed that the polarization signal measured over the ocean at the top of the atmosphere allows the observation of aerosols optical properties at visible wavelengths (e.g., 490 nm), regardless of the optical characteristics of the hydrosols (such as phytoplankton) (e.g., [43,50–52]). The third generation of the POLARization and Directionality of the Earth's Reflectances instrument (POLDER-3) on board the PARASOL (Polarization and Anisotropy of Reflectances for Atmospheric Science coupled with Observations from a Lidar) spacecraft has been the only recent satellite sensor that was able to perform multidirectional (up to 16 directions of observations) and polarized measurements over the ocean from space for several years (2005–2013). Thus, POLDER polarization signals have been used to determine the fine and coarse modes of aerosols, which are of great interest for improving our knowledge about the aerosol transport over the Atlantic ocean. Following the previous works of Harmel and Chami [43,52] about the capacity of polarized signal to significantly improve the aerosol type determination, the present paper focuses on the analysis of the transport of aerosols over the North Tropical Atlantic (NTA) Ocean in clear-sky conditions based on a time series of the total, fine and coarse AOD as derived from the polarized observations of POLDER/PARASOL satellite sensor. To this purpose, the POLAC (POLARization-based Atmospheric Correction) algorithm, which was developed for exploiting the polarized radiation measured from space [43], has been applied over the entire time series of POLDER/PARASOL data (2005–2013).

The paper is organized as follows. First, the quality and the accuracy of our satellite data is evaluated through comparisons of POLAC/PARASOL observations (i.e., POLDER/PARASOL observations processed by POLAC algorithm) with ground-based AERONET measurements, including the fine and coarse mode of aerosols. A qualitative comparison with MODIS AOD observations is also performed. Second, a climatology analysis of POLAC/PARASOL observations is carried out to examine the transport seasonal variability of the aerosols (total, fine and coarse modes) over the study area. Finally, the relevance of the AOD reanalyzed fields as provided by MACC [53] and MERRA-2 [54] models is discussed based on the POLAC/PARASOL observations.

2. Data and Method

2.1. Study Area

Many studies have documented the transport of large quantities of dust aerosols over the oceans from arid continental regions [55–57]. The current study focuses on the NTA ocean (Figure 1), which represents an area of particular interest to study the spatial and temporal variability of aerosols over the ocean due to its geographical position between the Western Africa (Sahara and Sahel) regions, which is the largest and most persistent dust source on Earth [6,18,58], and the coast of South America. While some of the dust aerosols emitted in Africa move southeastward in the direction of the Inter-Tropical Convergence Zone (ITCZ), the other significant part of the Saharan dust aerosols is deviated westward and carried by the SAL across the North Atlantic Ocean in direction of South-America [18]. In this study, we follow the spatial and temporal evolution of the saharan dust transport across the Atlantic ocean. Thus, the latitude range of our study area is delimited by 0°N–30°N. However, although dust aerosols likely represent the overwhelming majority of aerosols within the study area, sea salt aerosols, produced by wind friction over ocean surface, are also present [59]. Other aerosols having anthropogenic origin can also be detected such as biomass burning aerosols, typically from the Gulf of Guinea [18,60], or aerosols linked to fossil fuel combustion from urban areas. In order to further analyze more precisely the transport of aerosols over the NTA ocean, the study area has been divided into three sub-regions (Figure 1): the East zone (offshore Africa), which is delimited by 0°N–30°N and 10°W–30°W; the central zone (hereafter referred to as “centre zone”), which is delimited by 0°N–30°N and 30°W–45°W; the West zone (offshore Brazil), which is delimited by 0°N–30°N and 45°W–60°W. Note that Figure 1 also reports the location of the AERONET ground-based stations that are used in this study and the time average value of the aerosol optical depth (AOD) over the period 2005–2013 as observed by POLDER/PARASOL satellite sensor.

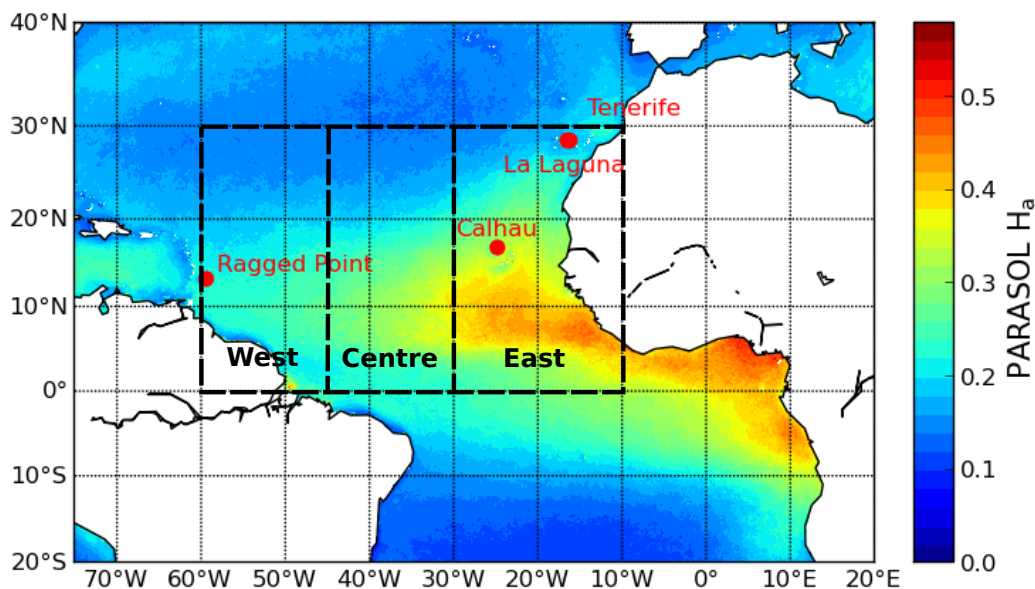


Figure 1. Map of the study area (North Tropical Atlantic Ocean), which is divided into 3 sub-regions: the West zone corresponds to the North East Brazilian zone, the East zone corresponds to the Africa zone and the Centre zone is located between these two zones. The color scale indicates the average value of the aerosol optical depth τ_n at 550 nm as derived from the POLAC/PARASOL satellite sensor time-series (2005–2013). The geographical location of the AERONET ground-based stations that are used in this study is also reported in the figure.

2.2. POLAC/PARASOL Observations

2.2.1. POLDER/PARASOL

The PARASOL satellite (CNES), which was operational from 2005 to 2013 within the A-Train constellation, carried the third generation of the POLDER sensor (POLDER-3). POLDER-3 is a passive optical imaging radiometer and polarimeter, which consists of a rotating wheel carrying filters that allow measurements at 9 wavelengths (443, 490, 565, 670, 763, 765, 865, 910 and 1020 nm). Three of the channels, namely 490 nm, 670 nm, 865 nm measure the polarization of the incident light. In addition to its ability to measure the polarization state of light, the POLDER-3 sensor is characterized by its wide field of view telecentric optics (114°) which allowed observation of the entire Earth's surface every 1 or 2 days at least. Interestingly, such a wide field of view also enabled observation of a given ground target along the satellite track at various viewing zenith angles, typically up to 16 directions of observation, thus permitting the measurements of the radiation coming from a target at different scattering angles. Note that due to signs of aging (notably its star tracker), the PARASOL satellite orbit moved off the A-train's track in December 2009 and its orbit was lowered 4 km below the A-Train from 2009. Since then, PARASOL orbit was continuously lowered until the end of the PARASOL mission. Such modification of the PARASOL orbit caused the temporal window of PARASOL to be delayed about 1 h at the end of 2010. A total number of 2939 PARASOL images acquired over the study area has been exploited here.

Over the oceans, the PARASOL operational algorithm [61] assumes non-absorbing particles, spherical or non-spherical particles. The size distribution of aerosols is modelled as a combination of two lognormal distributions, one in the fine mode (sub-micron size) and one in the coarse mode (effective radius typically larger than $1 \mu\text{m}$ [45,46]). POLDER/PARASOL products have already been assessed in Bréon et al. [41]. In Bréon et al. [41]'s study, an evaluation of the accuracy of different aerosol products derived from 5 sensors (POLDER, MODIS, MERIS, SEVIRI and CALIPSO) was made via a statistical comparison with AERONET data during a period of 5 years (March 2005–July 2010) on a global scale. It included the distinction between total and fine mode AOD. Their method revealed a good performance from POLDER with a correlation with AERONET around 0.9 for total AOD and 0.77 for fine mode AOD. It also showed that POLDER and MODIS retrievals are of similar quality over the ocean, even if the polarization-based retrieval using POLDER data offers a better fine mode estimate than MODIS. Finally, Bréon et al. [41] reported that the other satellite products are of lesser quality, strengthening our choice to use POLDER measurements.

2.2.2. Brief Overview of the POLAC Algorithm

To better exploit the multidirectional and polarization measurements made by POLDER-3, the POLAC atmospheric correction algorithm was developed (Harmel and Chami, 2011). The POLAC method uses as inputs the measurements of the multidirectional and polarized properties of the top of the atmosphere signal to retrieve atmospheric parameters, such as aerosol optical depth, fine and coarse modes of aerosol, and the water-leaving radiance over the ocean. To do so, the POLAC algorithm relies on the invariance of the POLDER/PARASOL radiance and polarization data to the concentration of in-water constituents (such as phytoplankton in open ocean waters), especially in the visible part of the spectrum such as 490 and 550 nm [50,52]. The POLAC algorithm is also built using an optimization scheme, which is based on the minimization of the Euclidian distance between the POLDER/PARASOL directional data, and on forward radiative transfer simulations in the coupled atmosphere-ocean system. Note that the POLAC method was preferred in this study to the so-called GRASP algorithm [62], which is also able to retrieve the aerosols properties from multidirectional and polarized satellite data, because of its consideration of the oceanic hydrosols optical properties during the inversion process.

For the purpose of this study, the Look Up Table (LUT), which is used to describe the aerosol models within POLAC algorithm, has been updated since the first version of POLAC algorithm

published in 2011. In particular, the absorption of the aerosols (fine and coarse modes) is taken into account. The non-spherical aerosol model that has been proposed by Volten et al. [63] and has been employed by Herman et al. [61], is used here as well. Note that such a non spherical model could be representative of dust-like aerosols. Table 1 reports the aerosol models used in the paper. The POLAC algorithm does not take into account potential variations of the vertical profile of aerosols. The vertical distribution of aerosols is modeled as exponentially decreasing with respect to the height, with 2-km scale height for both fine mode and coarse mode aerosols. Gordon [64] showed that the impact of the vertical distribution of aerosols (absorbing or not) on the top of atmosphere satellite reflectance is practically null in the near infrared spectrum independently of the aerosol amount and model. Since the POLAC algorithm uses the radiance measured by PARASOL in the near infrared band to derive the aerosol optical properties [43], the impact of the assumption using a fixed value of 2 km for the aerosol height scale should thus be weak. However, the POLAC algorithm also uses information measured in a visible band, namely 490 nm, coupled with the signal measured in the near infrared band. Duforêt et al. [65] showed that the vertical distribution of strongly absorbing aerosols could induce a maximum difference in the top-of-atmosphere unpolarized radiance up to 7% at 490 nm for a turbid atmosphere (aerosol optical depth value of 0.6) when the aerosol height scale value is fixed at 2 km (as in POLAC algorithm) and when the aerosols are located at an altitude of 4–5 km (such as dust-like aerosols) (see Table 1 in Duforêt et al. [65]). Such a difference could potentially lead to errors in the retrieval of aerosol properties by the POLAC algorithm. First, it should be highlighted that the POLAC algorithm uses the polarized radiance (i.e., Stokes parameter Q and U) at 490 nm, which is much weaker in magnitude than the unpolarized top-of-atmosphere radiance. Second, the radiance measured in the near infrared band remains the most sensitive band to derive aerosol properties at first order. Third, the validation of the POLAC-derived aerosol optical depth, which has been performed using ground-based AERONET measurements located at various contrasted sites, namely Capo-Verde (West Africa coast, dust-like aerosols), Lampedusa (Mediterranean Sea, urban aerosols) and Tahiti (Pacific Ocean, maritime aerosols), showed a satisfactory agreement as it could be observed in Harmel [66] (see omtab.obs-vlfr.fr/fichiers_PDF/Harmerl_PhD_09.pdf, Figure 4.12a). As a result, the POLAC derived aerosol products are reliable, at least for conditions where aerosols are not strongly absorbing, despite the assumptions made on the vertical distribution of aerosols.

Harmel [66] showed that the intrinsic uncertainty associated with the POLAC inversion of PARASOL signal is estimated at 0.5%, based on simulations. Then, Harmel and Chami [43] especially highlighted that the benefit of using multi-directional observations of a given target, as POLAC algorithm does, consists in providing reliable estimates of aerosol type, including the Ångström exponent that is calculated between 490 nm and 865 nm, with an uncertainty lower than 4%. POLAC is not the only algorithm to retrieve the fine and coarse fractions of POLDER-3 aerosol products over ocean. The operational level 2 POLDER-3 algorithm developed by Herman et al. [61] also discriminates these two modes over ocean and is employed by in Tanré [45], Tanré et al. [46] and more recently in Formenti et al. [67].

Our study is based on the use of AOD daily products retrieved by the POLAC algorithm during the lifetime of POLDER/PARASOL sensor, namely between March 2005 and September 2013. These data are derived at 550 nm at the ICARE Data and Service Centre (<http://www.icare.univ-lille1.fr>). It would have been interesting to compare these POLAC/PARASOL products to the operational level 2 POLDER-3 algorithm fine and coarse mode AOD retrievals products. However, such a work is beyond the scope of the current study.

In the rest of the paper, the notation “PARASOL AOD” is used for the total aerosol optical depth (i.e., fine mode AOD + coarse mode AOD) as observed by the POLDER/PARASOL sensor and retrieved by POLAC algorithm ; the notation “PARASOL AOD_f” is used to refer to the aerosol optical depth of the fine mode ; the notation “PARASOL AOD_c” is used to refer to the aerosol optical depth of the coarse mode. The fact that the fine and coarse mode of aerosol could be distinguished here in

PARASOL AOD is relevant for this study to identify the type of aerosols over the Atlantic Ocean and thus, to quantify the spatial distribution and transport of different types of aerosols.

Note that the 6 km resolution POLAC/PARASOL product was projected with conservative re-gridding onto a 25 km grid to correctly perform comparisons with MODIS observations and to investigate the relevance of MACC and MERRA-2 reanalysis products.

Table 1. Microphysical properties of the fine and the coarse modes of the spherical aerosol models used in this study by POLAC algorithm for the processing of PARASOL time-series data. The mean radius r_i , and the standard deviation σ_i are given in μm . The microphysical properties of the non-spherical model are not indicated in the table since its optical properties were directly obtained from laboratory measurements by Volten et al. [63].

Fine Mode			Coarse Mode		
Mean Radius r_i	Refractive Index	Standard Deviation σ_i	Mean Radius r_i	Refractive Index	Standard Deviation σ_i
0.04–0.08	1.45–0.0035i	0.46	0.75	1.33–0.001i	0.70
0.10–0.13				1.35–0.001i	
0.17				1.37–0.001i	

2.3. AERONET Ground Based Measurements

AERONET (AERosol RObotic NETwork) is an internationally federated ground-based instrument network of nearly 300 sites regularly reporting data, and over a thousand automatic sun and sky scanning Cimel (Cimel is NASA-AERONET's exclusive supplier of automatic Sun Sky Lunar photometers (CIMEL CE318-T) operating in near real time and providing aerosol optical and columnar microphysical properties.) radiometers, measuring and characterizing aerosol properties including aerosol optical depth [68]. Direct sun measurements are carried out in several spectral bands between 340 and 1640 nm to compute the total column atmospheric aerosol optical depth. Away from the Sun, measurements scan the sky and provide measurements of the radiation scattered down to the radiometer at 4 wavelengths, namely 0.44, 0.67, 0.87 and 1.02 μm , and over a wide range of scattering angles [69]. Then, sun and sky measurements are used to retrieve aerosol size parameters including the fraction of the fine and coarse mode of aerosol following the methodology of Dubovik et al. [70]. The AERONET inversion algorithm provides improved aerosol retrievals by fitting the entire measured field of radiances (i.e., the angular distribution of radiances and sun radiance) in the solar almucantar to a radiative transfer model. The inversion allows retrieval of the wavelength-dependent aerosol complex index of refraction and the bimodal particle size distribution in the size range [0.05–15 μm], which enables calculations of aerosol properties [70]. The AOD processing includes the spectral de-convolution algorithm (SDA) described in O'Neill et al. [71]. This algorithm provides fine (sub-micron size) and coarse (super-micron size) AOD at 500 nm. The algorithm fundamentally assumes that the coarse mode Angström exponent and its derivative are close to zero. Its advantage is based on the fact that it produces useful indicators of aerosol size discrimination at the frequency of extinction measurements. In this paper, the level 2.0 quality-assured AERONET SDA retrievals (Version 2) derived at 500 nm are used. In order to compare AERONET AOD products to other data sets at the same wavelength, AERONET derived AOD products at 500 nm are interpolated to determine AERONET derived AOD products at 550 nm following Angström power law:

$$\tau_{550} = \tau_{500} \left(\frac{500}{550} \right)^\alpha \quad (1)$$

where τ_{550} is the AOD or AOD_f at 550 nm, τ_{500} is the AOD or AOD_f at 500 nm and α is the Angström exponent of the AOD or AOD_f at 500 nm.

The AERONET AOD products at 550 nm are referred to as "AERONET AOD" for total aerosol optical depth, "AERONET AOD_f " for the fine mode aerosol optical depth and "AERONET AOD_c " for

the coarse mode aerosol optical depth. To ensure their quality, the AERONET products have undergone pre-field and post-field calibration as provided by AERONET quality assurance program ; they have been cloud cleared and manually inspected as well. The typical overall uncertainty in the AERONET AOD data for field instruments is about ± 0.01 to ± 0.02 [72,73]. To verify the accuracy of PARASOL AOD values, near-continuous and long-term data sets of AERONET AOD, AERONET AOD_f and AERONET AOD_c as provided by the following four AERONET stations (<https://aeronet.gsfc.nasa.gov/>) from 2005 to 2013 were processed: Santa Cruz Tenerife (28.47°N, 16.25°W), La Laguna (28.48°N, 16.32°W), Calhau (16.86°N, 24.87°W) and Ragged Point (13.17°N, 59.43°W) (Figure 1) are used. Note that continental AERONET stations located over the study area, such as Dakar, Bambey or Dahkla, cannot be used since PARASOL AOD products derived by POLAC method are delivered over the ocean only. Cape Verde and Guadeloupe AERONET stations are also not used for evaluating POLAC retrievals because of the lack of available data. Therefore, the POLAC aerosol products may not be sufficiently accurate to compare with these AERONET sites, including the Dakar site which has one of the longest data records. Note also that the AERONET stations are spatially distributed so as to cover the various sub-regions of the study area.

From 2005 to 2010, AERONET AOD data were selected every day during a 3-hour time window centered on the approximate revisit time of PARASOL satellite, namely at 14:30 UTC in the East zone and at 17:30 UTC in the West zone. From 2011 to 2013, the approximate revisit time of PARASOL satellite is shifted to 3:30 pm in the East zone and to 6:30 pm in the West zone to compensate the continuing loss in orbit of PARASOL satellite as mentioned in Section 2.2. The AERONET AOD data are then daily averaged prior to comparing with daily PARASOL AOD products.

2.4. Aerosol Properties Derived from Global Reanalysis

2.4.1. MACC Reanalysis

Since 2003, the European Center for Medium-Range Weather Forecasts (ECMWF) performed a reanalysis of global atmospheric composition, the so-called “Monitoring Atmospheric Composition and Climate (MACC) Reanalysis”. Using the aerosol size as a proxy for aerosol origin, MACC reanalysis includes aerosol optical depths that are divided into three classes: anthropogenic, mineral-dust and sea-salt. The MACC reanalysis database is constructed by assimilating satellite data at several spectral bands (including 550 nm) into the ECMWF Integrated Forecast System (IFS) global model. Current MACC aerosol reanalysis are performed using an aerosol data assimilation system developed by Morcrette et al. [74] and Benedetti et al. [75] which relies on MODIS AOD measurements and a 4D-Var approach. The spatial resolution of the MACC reanalysis data set is about 80 km on 60 vertical levels from the surface up to approximately 65 km. The MACC-II VAL sub-project validated the outputs of the reanalysis but several quality issues remain such as those regarding the sea salt aerosol mixing ratio above freshwater or changes in biomass burning emissions for example (<https://software.ecmwf.int>) [76,77]. In this study, MACC total aerosol optical depth monthly mean at 550 nm, hereafter referred to as MACC AOD, is compared with the corresponding PARASOL AOD measurements over the time period 2005–2013. The fact that MACC reanalysis is able to distinguish between aerosol origins is important to gain understanding on the fine mode and coarse mode aerosol transport over the NTA ocean.

2.4.2. MERRA-2 Reanalysis

The Modern-Era Retrospective analysis for Research and Applications, Version 2 (MERRA-2), developed by NASA’s Global Modeling and Assimilation Office (GMAO), is the latest atmospheric reanalysis of the satellite era (1980 onward) produced using the Goddard Earth Observing System (GEOS-5) atmospheric model, data assimilation system version 5.12.4 [54,78,79] and the three-dimensional variational data analysis (3DVAR) Gridpoint Statistical Interpolation (GSI) meteorological analysis scheme [80,81]. GEOS-5 model spatial resolution is roughly 50 km in the

latitudinal direction with 72 hybrid-eta layers from the surface to approximately 65 km. Most products are delivered on the standard $0.5^\circ \times 0.625^\circ$ latitude by longitude grid [82]. In comparison with the original first version of MERRA, MERRA-2 includes an aerosol analysis as described in Randles et al. [82,83]. To assimilate AOD at 550 nm, an analysis splitting technique is used in which a two-dimensional analysis is achieved using error covariances derived from innovation data [82]. Then, horizontal increments are projected vertically and across species via an ensemble method [54]. New AOD observations are assimilated from several sources, including:

- reflectances from AVHRR (1979–2002, ocean only);
- reflectances from MODIS (2000–present);
- AOD retrievals from MISR (2000–2014, bright, desert regions only);
- direct AOD measurements from the ground-based AERONET (1999–2014).

MERRA-2 reduces spurious jumps and trends associated with changes in the meteorological observing system [84]. Using recent developments at GMAO in the field of modeling and data assimilation, MERRA-2 is now able to combine assimilation systems for land, ocean, atmosphere and chemistry. As an example, MERRA-2 includes aerosol data assimilation that can interact with atmospheric radiative processes and thus provides a multidecadal reanalysis in which aerosol and meteorological observations are jointly assimilated within a global data assimilation system [54]. In order to compare with PARASOL AOD data, different types of MERRA-2 monthly mean products at 550 nm were used here: the Total Aerosol Extinction AOD (hereafter referred to as “MERRA-2 AOD”), the Dust Extinction AOD-PM 2.5 and the Sea Salt Extinction AOD-PM 2.5 (PM 2.5, i.e., the mass concentration of aerosols with diameters less than 2.5 μm). Note that even though dust and sea salt aerosols mostly contribute to the coarse mode AOD, they could be also present within the fine mode fraction. In that sense, unlike MACC reanalysis, the fine mode of AOD due to primary dust and sea-spray are available in the MERRA-2 reanalysis products. To directly compare fine mode AOD to the PARASOL AOD_f product, it is necessary to sum both MERRA-2 fine modes aerosol products, namely the Dust Extinction AOT-PM 2.5 and the Sea Salt Extinction AOT-PM 2.5 products, to get the total fraction of the fine mode of aerosols. Such a sum is hereafter referred to as “MERRA-2 AOD_f”. The fraction of coarse mode of MERRA-2 AOD products, hereafter referred to as “MERRA-2 AOD_c”, is calculated by subtracting MERRA-2 AOD_f to MERRA-2 AOD product.

As for POLAC/PARASOL product, MACC (80 km spatial resolution) and MERRA-2 (50 km spatial resolution) AOD products used in this study were projected onto the same 25 km grid in conservative projection. Such a projection aims at making consistent the analysis of MACC data set, MERRA-2 data set and PARASOL data set.

3. Results

3.1. Evaluation of PARASOL AOD Retrievals

3.1.1. Comparison with AERONET Measurements

PARASOL AOD products (total, fine and coarse modes) (Section 2.2) are evaluated with respect to AERONET measurements (Section 2.3) from 2005 to 2013. To compare with AERONET ground-based measurements, the highest spatial resolution of PARASOL AOD products (i.e., 6 km) has been used.

Figure 2 shows the monthly time series of the total AOD difference between PARASOL observations and corresponding ground-based measurements acquired by the four selected AERONET stations (Figure 1).

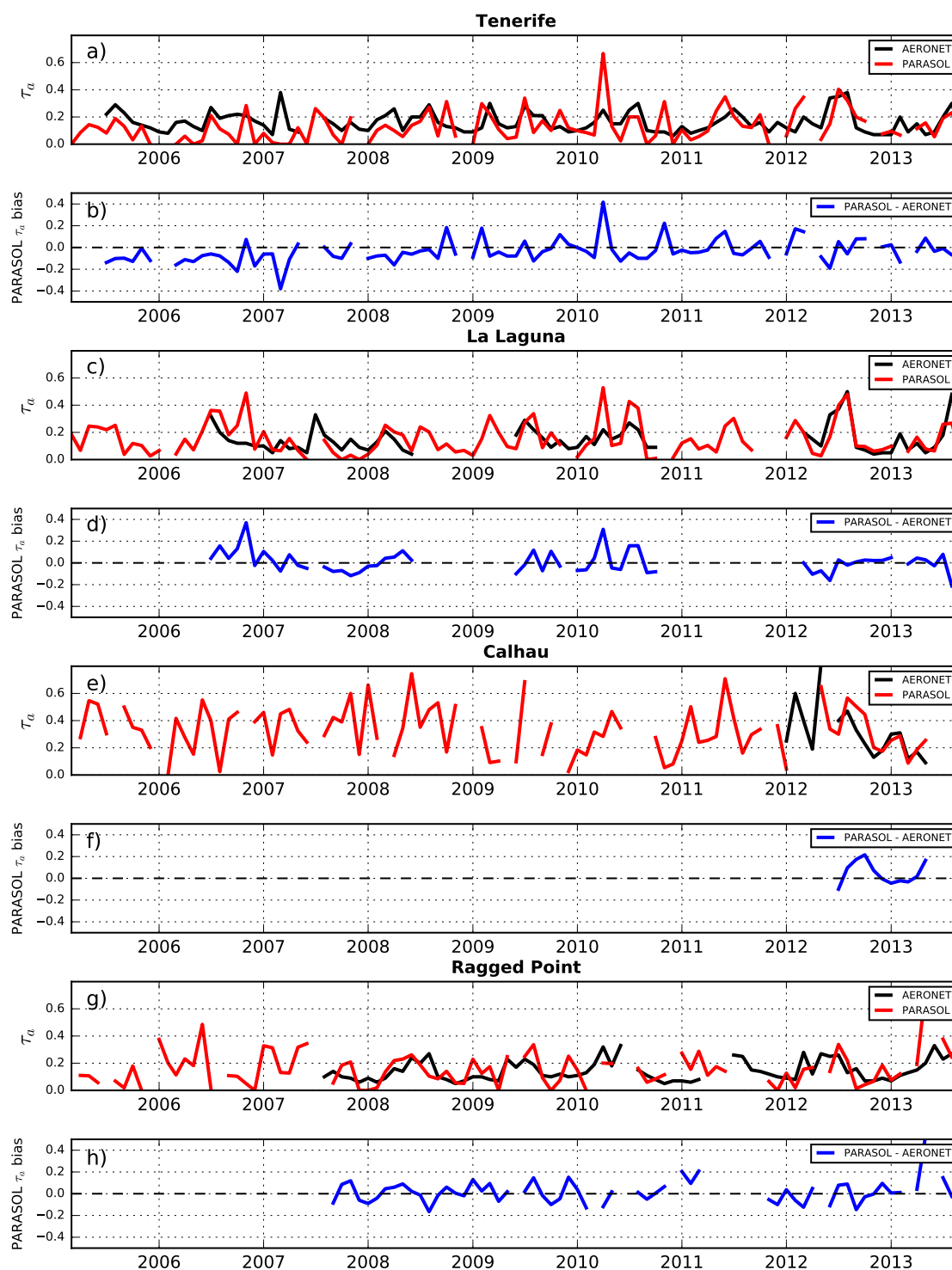


Figure 2. Comparisons of the total AOD (i.e., fine + coarse mode) monthly mean at 550 nm between PARASOL observations (red point) and AERONET measurements (black curve) from 2005 to 2013: (a) Tenerife, (c) La Laguna, (e) Calhau and (g) Ragged Point. Corresponding PARASOL AOD bias with respect to AERONET AOD: (b) Tenerife, (d) La Laguna, (f) Calhau and (h) Ragged Point.

First, AERONET AOD values exhibit a seasonal variability with highest AOD values (between 0.2 and 0.4 at 550 nm depending on the station) in summer (June–July–August) and minimum AOD values below 0.1 in winter (December–January–February) at almost all stations. It is particularly noticeable

at Tenerife (Figure 2a) and La Laguna (Figure 2c), sites located near the West Africa coast where the highest AERONET AOD values (over 0.3) are observed. Such seasonal variability is likely due to mineral dust advection during large Saharan dust outbreaks occurring in summer since we can observe the same but less pronounced seasonal variability in AERONET AOD_c (Figure 4). At Ragged Point, the most westerly station of the study area, the seasonal variability remains observable despite an attenuation illustrated by an annual amplitude around 0.1 (Figure 2g). Unlike other stations in the East zone, the almost total lack of high daily AOD values over 0.4 (not shown) leads to the observed lower AOD variability, which is probably due to dry and wet removal processes of dust aerosols during the transport across the Atlantic Ocean. The seasonal variability is not the only temporal variability experienced by the aerosol optical depth. Because of the high frequency and intensity of aerosol production in North Africa associated with high temporal variability of meteorological parameters (precipitations, wind,...), AERONET AOD shows an important daily variability as illustrated by the high AERONET standard deviation values compared to corresponding AERONET AOD (Table 2).

Second, the comparison between the two data sets presented by Figure 2 and Table 2 show that, at all stations, PARASOL AOD values are in a good agreement with the AERONET AOD temporal variability. Yet, some discrepancies are observed with most of the biases ranging from -0.2 to 0.2 , which is a consistent range based on previous studies [85,86]. Outside the bias range $[-0.2; 0.2]$, PARASOL biases are mostly positive, which may be explained by an occasional failure in the detection of clouds [87]. In Calhau, discrepancies between PARASOL and AERONET retrievals in the SON period, as reported in Table 2, are obtained from measurements only over one season (SON 2012) thus limiting the significance of the results.

Figures 3 and 4 present similar comparisons as Figure 2, but for the fine and coarse modes of aerosols respectively. Note that such a study is unusual as most of studies referring to spatial and temporal variability of aerosols are focused on the evaluation of the total AOD without making any specific distinctions between the fine and coarse modes of aerosols. While the comparison of PARASOL AOD_c with AERONET measurements shows a satisfactory agreement with low biases at all stations (Figure 4, Table 2), PARASOL AOD_f presents weaker values. An overestimation of AOD_f is observed in PARASOL (Figure 3, Table 2), with high biases $[-0.2; 0.2]$ compared to AERONET AOD_f value range $[0; 0.2]$. This is particularly noticeable at Ragged Point (Figure 3g,h) where daily mean PARASOL AOD_f can be twice as high as daily mean AERONET AOD_f (Table 2). The cause of the overestimation of the AOD_f observed by POLDER/PARASOL might be due to the fact that fine mode aerosols are more difficult to observe due to their size, which implies an increase of errors in satellite observations. Figure 3 and Table 2 also show that values of AERONET AOD_f are much lower than total AOD values (Figure 2): AOD_f maxima are typically lower than 0.2 (Figure 3a,c,e,g). On the contrary, AERONET AOD_c values are high, typically in the range between 0 and 0.4 (Figure 4), and can even reach total AOD values at some points. These observations point out the lower contribution of the fine mode and the opposite high contribution of the coarse mode to the total extinction. Such a result is consistent with the study made by Schutz [88] that revealed significant concentrations of coarse mode of dust close to source regions. As a consequence of the reduced number of the fine mode of aerosols, the seasonal and daily variabilities of AERONET AOD_f is significantly reduced (Figure 3), while those of the coarse mode still exist but are less pronounced (average of maximum values around 0.3, Figure 4) than total AOD variabilities.

Figure 5 shows the results from a statistical analysis that has been performed between PARASOL and AERONET for the total, fine and coarse AOD. It should be highlighted that the relatively small number of coincident AERONET and PARASOL data could be explained by the constraints used to ensure a consistent comparison. In particular, only AERONET AOD data that are measured within a 3-h time window centered on the approximate revisit of PARASOL satellite have been selected, as mentioned in Section 2.3, rather than all AERONET data available over the course of the day.

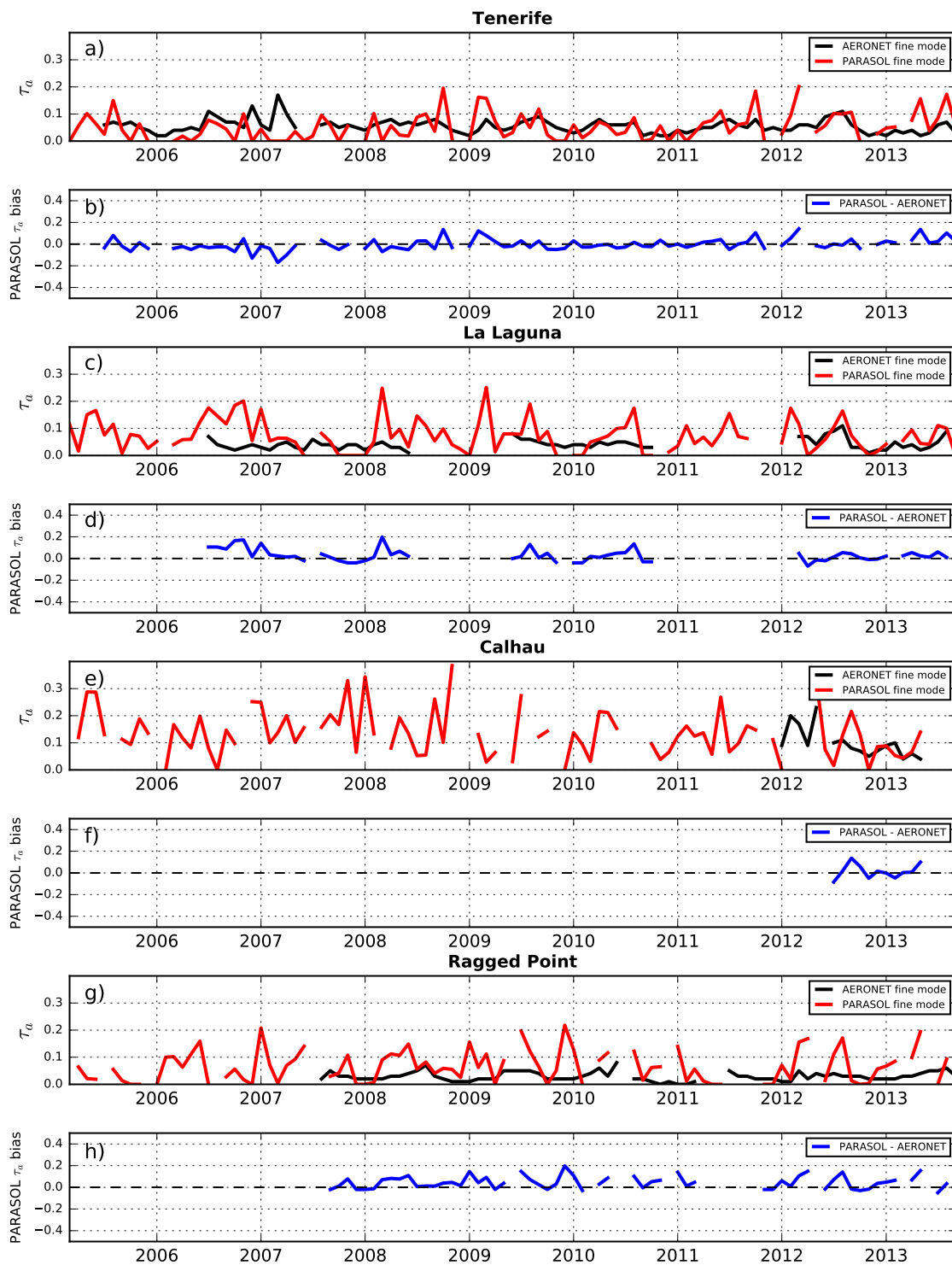


Figure 3. Similar as Figure 2 but for AOD_f (fine mode of aerosols): (a) Tenerife, (c) La Laguna, (e) Calhau and (g) Ragged Point. Corresponding PARASOL AOD_f bias with respect to AERONET: (b) Tenerife, (d) La Laguna, (f) Calhau and (h) Ragged Point.

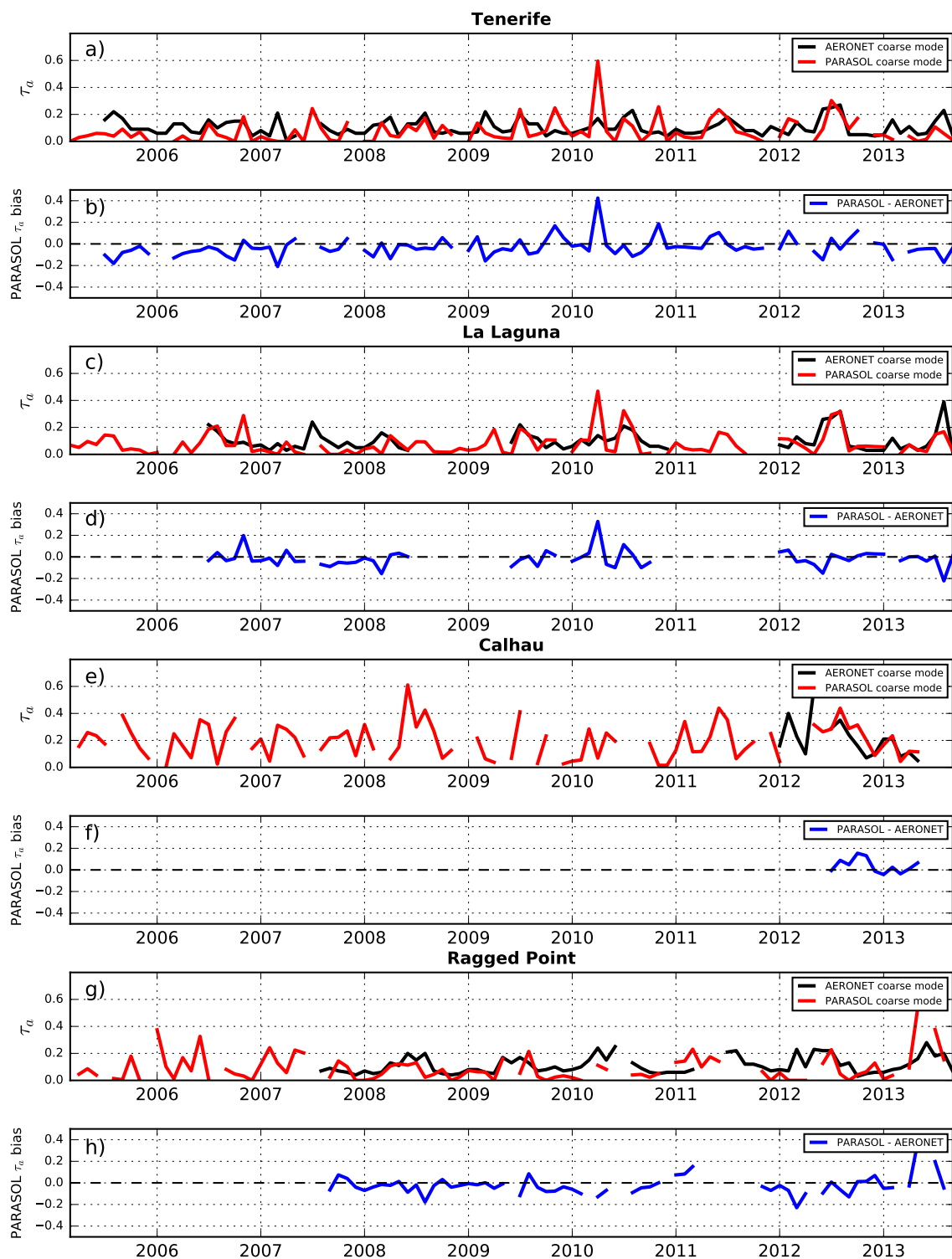


Figure 4. Similar as Figure 2 but for AOD_c (coarse mode of aerosols): (a) Tenerife, (c) La Laguna, (e) Calhau and (g) Ragged Point. Corresponding PARASOL AOD_c bias with respect to AERONET: (b) Tenerife, (d) La Laguna, (f) Calhau and (h) Ragged Point.

PARASOL observations of both AOD and AOD_c exhibit satisfactory correlation coefficients (greater than 0.74) and low biases ranging from -0.03 to 0.03 at all AERONET stations (Figure 5a,c,d,f,g,i,j,l). Such results indicate that the location of the stations, from East to West zone, has a low impact on PARASOL scores and the discrepancies shown in Figure 5 do not appear

increase with increasing AOD. Note that the higher number of AOD_c observations (120) compared to AOD and AOD_f observations (108) in La Laguna (Figure 5d–f) is due to the lack of Angström exponent observations for the total and the fine mode (coarse mode Angström exponent is set to 0 for the La Laguna site), while observations of AOD products exist.

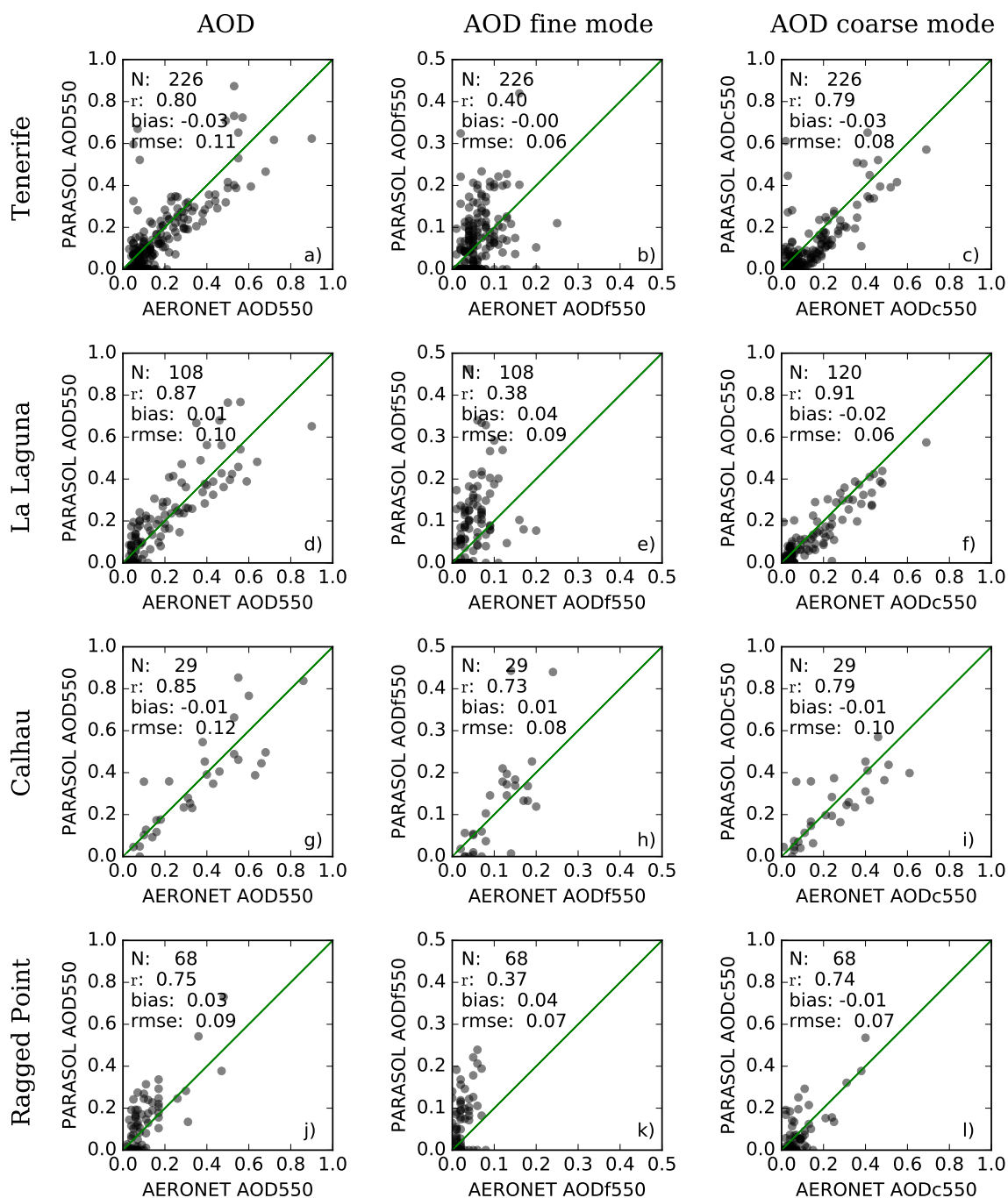


Figure 5. Left column: comparisons of PARASOL AOD and AERONET AOD at 550 nm for the period 2005–2013 at (a) Tenerife, (d) La Laguna, (g) Calhau and (j) Ragged Point. Center column: same comparisons as left column but for AOD_f at (b) Tenerife, (e) La Laguna, (h) Calhau and (k) Ragged Point. Right column: same comparisons as left column but for AOD_c at (c) Tenerife, (f) La Laguna, (i) Calhau and (l) Ragged Point.

In parallel, PARASOL AOD_f presents the lowest performance with correlation coefficients between 0.37 and 0.73, and biases ranging from 0.00 to 0.04 (Figure 5b,e,h,k). At Tenerife, the low correlation coefficient (0.40) associated with zero bias can be explained by the compensation between both negative and positive bias which tends to get an average close to 0. Figure 5 also shows that, while PARASOL AOD_f biases are positive, PARASOL AOD_c are negative, a trend that has also been seen in Table 2. This may lead to a slight underestimation of the coarse mode AOD and an overestimation of the fine mode AOD from PARASOL. Different studies have already shown that in situ observations often lead to significantly larger mean particle sizes than retrievals from remote sensing instruments, thus impacting the coarse mode size distribution [89–92]. It may explain the slight underestimation of PARASOL AOD_c. The cause of this discrepancy is still unknown. Kleidman et al. [69] suggested that it may come from some ambiguity in the definition of the radius-threshold for fine and coarse mode between the sunphotometer and the satellite products [69].

Despite the possible accumulation of several error sources such as the difference in the spatial resolution between ground-based and satellite data sets (6 km for the PARASOL AOD against few meters for the AERONET AOD) and such as occasional errors in ground based measurements and the PARASOL cloud detection, PARASOL shows a good performance in the observation of the total and coarse mode AOD over the NTA ocean. The satisfactory performance of PARASOL total AOD is also consistent with Harmel [66] on POLAC inversion made on PARASOL AOD (Section 2.2.2). Our analysis therefore highlights the ability of PARASOL to detect the contribution of coarse aerosols, and to a lesser extent, fine aerosols to the total AOD which are innovative contributions over such a region.

Table 2. AOD/ σ (standard deviation)/number of observations from PARASOL observations and AERONET measurements at 550 nm averaged from 2005 to 2013.

		DJF	MAM	PARASOL JJA	SON	An
Total	Tenerife	0.09/0.14/44	0.09/0.14/64	0.16/0.19/118	0.12/0.12/54	0.13/0.16/280
	La Laguna	0.10/0.10/47	0.14/0.14/81	0.26/0.18/106	0.10/0.11/40	0.17/0.16/274
	Calhau	0.27/0.23/45	0.31/0.20/57	0.40/0.20/44	0.39/0.18/45	0.34/0.21/191
	Ragged Point	0.15/0.14/36	0.19/0.14/43	0.23/0.17/27	0.10/0.11/44	0.16/0.15/150
Fine mode	Tenerife	0.04/0.06/44	0.04/0.07/64	0.06/0.07/118	0.05/0.07/54	0.05/0.07/280
	La Laguna	0.05/0.07/47	0.08/0.09/81	0.11/0.08/106	0.05/0.07/40	0.08/0.09/274
	Calhau	0.13/0.13/45	0.13/0.10/57	0.12/0.09/44	0.16/0.12/45	0.13/0.11/191
	Ragged Point	0.07/0.08/36	0.08/0.06/43	0.09/0.08/27	0.04/0.05/44	0.07/0.07/150
Coarse mode	Tenerife	0.05/0.09/44	0.05/0.10/64	0.10/0.15/118	0.06/0.08/54	0.07/0.12/280
	La Laguna	0.05/0.06/47	0.06/0.10/81	0.15/0.14/106	0.05/0.07/40	0.09/0.12/274
	Calhau	0.14/0.14/45	0.18/0.13/57	0.28/0.16/44	0.23/0.14/45	0.20/0.15/191
	Ragged Point	0.08/0.10/36	0.11/0.13/43	0.14/0.13/27	0.06/0.07/44	0.09/0.11/150
		DJF	MAM	AERONET JJA	SON	An
Total	Tenerife	0.11/0.11/420	0.16/0.18/427	0.24/0.23/589	0.14/0.11/489	0.17/0.18/1925
	La Laguna	0.09/0.11/144	0.13/0.14/199	0.25/0.24/306	0.11/0.08/170	0.16/0.19/819
	Calhau	0.28/0.33/66	0.23/0.24/95	0.45/0.17/30	0.24/0.18/56	0.27/0.26/247
	Ragged Point	0.09/0.04/294	0.16/0.10/257	0.24/0.15/239	0.10/0.07/306	0.14/0.11/1096
Fine mode	Tenerife	0.04/0.04/420	0.06/0.06/427	0.07/0.05/589	0.06/0.04/489	0.06/0.05/1925
	La Laguna	0.03/0.03/144	0.04/0.03/199	0.05/0.05/306	0.04/0.02/170	0.04/0.04/819
	Calhau	0.10/0.10/66	0.09/0.08/95	0.11/0.03/30	0.07/0.03/56	0.09/0.08/247
	Ragged Point	0.02/0.02/294	0.03/0.02/257	0.05/0.03/239	0.02/0.02/306	0.03/0.02/1096
Coarse mode	Tenerife	0.07/0.08/420	0.10/0.13/427	0.16/0.18/589	0.08/0.09/489	0.11/0.13/1925
	La Laguna	0.06/0.07/203	0.08/0.10/230	0.18/0.19/339	0.07/0.07/227	0.11/0.14/999
	Calhau	0.19/0.23/66	0.14/0.17/95	0.33/0.13/30	0.17/0.15/56	0.18/0.19/247
	Ragged Point	0.07/0.03/294	0.13/0.08/257	0.19/0.13/239	0.08/0.06/306	0.11/0.09/1096

3.1.2. Comparison with MODIS Satellite Observations

Figure 6 and Table 3 compare the AOD, AOD_f and AOD_c between PARASOL observations and the Level-3 MODIS Atmosphere Monthly Global Product MYD08_M3 collected from the Aqua platform (<https://modis-atmos.gsfc.nasa.gov/products/monthly>), averaged from 2005 to 2013. Note that the use of MISR satellite sensor products [93], which has a finer spatial resolution (4.4 km) than MODIS would have been interesting. However, the goal of this paper is not to compare all the size-resolved AOD products and the use of MODIS data was preferred here, in particular because the MACC and MERRA-2 reanalysis aerosol datasets used in this paper are based on the assimilation of MODIS data. Since PARASOL AOD products derived by POLAC method are not delivered over the land, this study only uses MODIS products over the ocean. It also should be highlighted that the Multi-Angle Implementation of Atmospheric Correction (MAIAC), which is designed to work with MODIS data to facilitate deriving both aerosol and land surface reflectance products, is a relevant method [94] that has not been used here since our study deals with data collected over the ocean surface.

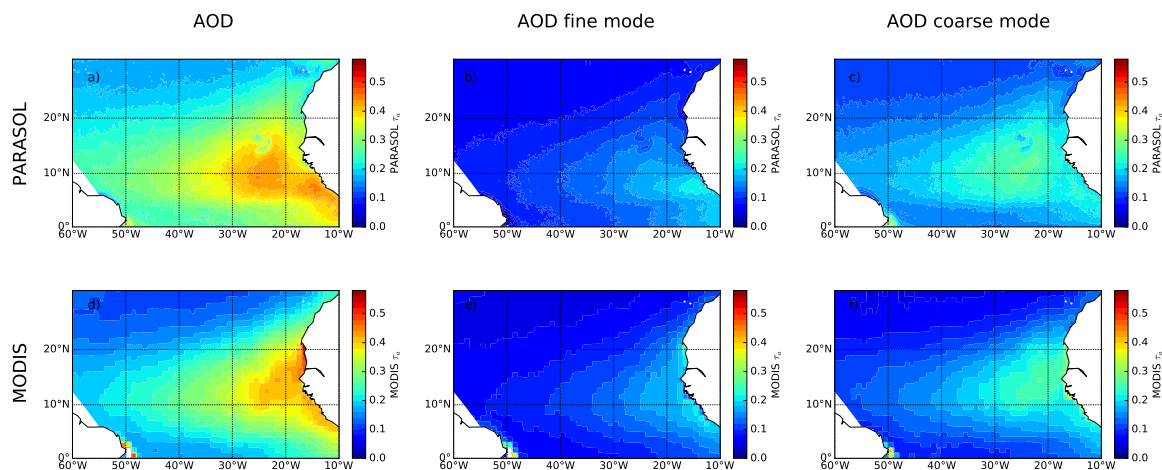


Figure 6. Spatial distribution of the total AOD (left column), AOD_f (central column) and AOD_c (right column) observed by PARASOL satellite (top figures (a–c)) and MODIS satellite (bottom figures (d–f)) at 550 nm averaged from 2005 to 2013. Note that the Level-3 MODIS Atmosphere Monthly Global Product MYD08_M3 collected from the Aqua platform (<https://modis-atmos.gsfc.nasa.gov/products/monthly>) has been used.

In this study, PARASOL coarse mode aerosols are defined by an effective radius larger than 1 μm while MODIS coarse mode aerosols are defined by an effective radius larger than 0.98 μm (https://modis.gsfc.nasa.gov/data/atbd/atbd_mod02.pdf). Our results show that PARASOL and MODIS data agree reasonably well. For both of them, the AOD decreases by a factor of ~ 1.5 (Table 3) from the coast of North Africa westward to the Caribbean Sea, presumably due to wet and dry depositions of mineral dust during transport and horizontal spreading. However, a few differences between PARASOL and MODIS do exist. First, the transport of aerosols over the NTA ocean seems to be less strong in MODIS observations with a horizontal dispersion of aerosols that is not as extended as PARASOL transport (Figure 6a,d) which is illustrated by total AOD values equal to 0.18 for MODIS against 0.23 for PARASOL in the West sub-region (Table 3). This can be explained by the lower amount of coarse mode aerosols observed by MODIS, especially in the West sub-region (Figure 6c,f, Table 3), which implies a decrease of MODIS total AOD over the study area, and more specifically over the West sub-region. Second, the highest AOD values derived from MODIS off the coast of Mauritania (Africa) are observed further southward with PARASOL observations, both for AOD and AOD_f products, and to a lesser extent in AOD_c. Usually, important features of AOD along the coast of the Gulf of Guinea are often attributable to biomass burning aerosols, but large amounts of dust aerosols, transported from sources further inland, could also be present. It may indicate that biomass burning aerosol

is not well observed using POLDER/PARASOL sensor, as indicated by the largest bias between PARASOL AOD_f and MODIS AOD_f found in winter (0.03) in regard to other seasons. Perhaps, this is because of a less strict PARASOL cloud mask which leads to overestimated AOD values by PARASOL. The area off the coast of Mauritania is also subjected to a coastal upwelling where strong winds blow across the surface of the ocean thus making surface waters diverge horizontally [95]. In such area, the differences observed between POLDER/PARASOL and MODIS sensors could possibly come from discrepancies between the inversion algorithms used for each sensor, such as the wind retrieval algorithm. In particular, a different whitecap coverage (a parameter that is function of the wind speed), the stability of the lower atmosphere and changes in the sea-surface temperature could impact the observed apparent microwave temperature and short-wave albedo of the sea surface [96], thus leading to different observations of AOD between both satellite sensors.

Table 3. Total AOD, AOD_f , AOD_c at 550 nm from PARASOL observations, MODIS observations, MERRA-2 reanalysis and MACC reanalysis averaged from 2005 to 2013.

		Total			Fine Mode			Coarse Mode		
		East	Center	West	East	Center	West	East	Center	West
PARASOL	DJF	0.34	0.27	0.21	0.16	0.11	0.08	0.18	0.16	0.13
	MAM	0.35	0.29	0.25	0.13	0.11	0.09	0.22	0.18	0.16
	JJA	0.35	0.30	0.28	0.14	0.11	0.10	0.21	0.19	0.18
	SON	0.27	0.23	0.19	0.11	0.09	0.07	0.16	0.14	0.12
	An	0.33	0.27	0.23	0.14	0.10	0.08	0.19	0.17	0.15
MODIS	DJF	0.30	0.20	0.14	0.13	0.09	0.06	0.17	0.11	0.08
	MAM	0.32	0.23	0.19	0.12	0.08	0.07	0.20	0.15	0.12
	JJA	0.34	0.26	0.23	0.13	0.10	0.09	0.21	0.16	0.14
	SON	0.22	0.16	0.15	0.10	0.07	0.08	0.12	0.09	0.07
	An	0.30	0.22	0.18	0.12	0.09	0.08	0.18	0.13	0.10
MERRA-2	DJF	0.27	0.17	0.12	0.10	0.06	0.04	0.17	0.11	0.08
	MAM	0.28	0.19	0.16	0.14	0.08	0.06	0.14	0.11	0.10
	JJA	0.29	0.21	0.19	0.14	0.09	0.08	0.17	0.12	0.11
	SON	0.20	0.15	0.12	0.08	0.05	0.04	0.12	0.10	0.08
	An	0.26	0.18	0.15	0.11	0.07	0.06	0.15	0.11	0.09
MACC	DJF	0.27	0.22	0.16						
	MAM	0.25	0.30	0.25						
	JJA	0.32	0.27	0.24						
	SON	0.23	0.20	0.17						
	An	0.29	0.23	0.20						

Despite the overestimation of PARASOL AOD_f observed in the comparison with AERONET measurements, the fine mode of PARASOL shows a good consistency with MODIS AOD_f (Figure 6b,e and Table 3). This may indicate the difficulty to derive size information from the spectral and directional reflectance [41]. Kalashnikova and Kahn [36] also point out that low optical depths (below 0.5), that are predominant in fine mode AOD, combined with assumptions made in the satellite retrieval algorithms about ocean surface optical properties (reflectance and emissivity) [97], may lead to an overestimation of the AOD in MODIS. This could be the case as well in PARASOL.

Finally, the overall satisfactory comparison between PARASOL AOD observations and MODIS dataset confirms that POLDER/PARASOL sensor is relevant to study the transport of aerosol over the NTA ocean.

3.2. Seasonal Variability and Climatology of AOD Observed by PARASOL

Aerosol production in North Africa and exportation over the NTA ocean is characterized by a pronounced seasonal evolution [98,99]. To analyze the seasonal variability, Figure 7 presents the climatology of PARASOL products (AOD , AOD_f , AOD_c) at 25 km spatial resolution for each season

and averaged over the whole time series 2005–2013. At seasonal scale, the production of different types of aerosols coming from different regions of Africa leads to both a spatial and temporal variability of the amount of aerosols in the atmosphere [56]. Thus, seasonal changes in spatio-temporal aerosol activity are correlated with seasonal changes in local meteorological conditions providing favorable atmospheric conditions for aerosol emission (e.g., [100]). Most of the aerosol variability comes from spatio-temporal dust production and, to a lesser extent, from biomass burning aerosols production. For the latter, even if vegetation fires could occur over the course of the entire year in Sub-Saharan Africa, fires are infrequent during the wet season. Therefore, the largest amount of biomass burning aerosols are emitted from the Gulf of Guinea in equatorial Africa during the dry season [101] and thus, part of the winter plume over the NTA ocean is due to smoke (Figure 7a). This variability is mainly driven by the oscillation of the ITCZ leading to the succession of two meteorological regimes over the Sahel during the year [102]: during summer, the Sahel is submitted to the wet monsoon flow from South-West due to the northern shift of the ITCZ. An occurrence of extremely high daily concentrations of dust is induced by strong surface winds associated to Mesoscale Convective Systems that cross the Sahel. On the opposite side, in winter, the northeastern dry Harmattan winds allow a Saharan dust transport towards the Gulf of Guinea. This changeover explains the south-north migration of the main transport corridor for the aerosol outflow from Africa observed in Figure 7: from under 15°N in winter (Figure 7a), with the plume extending to South America, to 10°N – 30°N in summer (Figure 7g) with an export into the Caribbean and toward Florida [103–105]. In spring, the amount of aerosols reaches its maximum with PARASOL AOD greater than or equal to 0.6 near the coast of Africa and over 0.4 at 40°W (Figure 7d) due to the highest values of PARASOL AOD_c in this season (Figure 7f, Table 3). In summer, PARASOL AOD increases in the Centre zone and especially in the West zone, showing the highest transport of aerosol across the ocean over the year (Figure 7g, Table 3). This result from a summer transport at higher elevations (up to 7 km) within the SAL combined with higher wind speeds compared to winter transport [92,106]. In autumn, a significant decrease of PARASOL AOD appears with values lower than 0.4 over the entire domain (Figure 7j) marking the end of the summer intensive period of aerosol transport over the NTA ocean.

Consistent features are found for PARASOL AOD_c with lower values (Figure 7, right column): PARASOL AOD_c varies between 0.1 and 0.4 whereas PARASOL AOD can reach 0.6 according to season. High values of PARASOL AOD_c that are observed over 10°N also confirm the important part of the coarse mode in the dust aerosols coming from the SAL. Such results attest that the aerosol spatio-temporal variability is primarily under the influence of coarse dust aerosol spatio-temporal variability and show that the major contribution of the aerosol coarse mode, already observed in Section 3.1.1 at four AERONET stations, is found over the entire study area.

Regarding the fine mode of PARASOL AOD, Figure 7 (middle column) and Table 3 show values below 0.3 throughout the year and presents some differences in spatio-temporal variability with the coarse mode AOD and thus, with the total AOD. First, PARASOL AOD_f maximum value is reached in winter where the aerosols originate from the equatorial Africa (Figure 7b); second, PARASOL AOD_f observed in summer at equatorial Africa also prevails over PARASOL AOD_f that originates from the North of Africa, despite the high emission of aerosols at this period of the year (Figure 7h). Such an observation suggests that an important source of PARASOL AOD_f is located in equatorial Africa. Since biomass burning aerosols are mainly found in this area, it does thus make sense to believe that biomass burning aerosols are composed of fine mode aerosols. However, it should be highlighted that the aerosols used in the POLAC algorithm are not as absorbing as biomass burning aerosols can be. As a result, the occurrence of biomass burning aerosols could alter significantly the performance of POLAC retrieval. PARASOL AOD_f and PARASOL AOD_c are also differentiated by their transport over the ocean. While PARASOL AOD_f is fairly zero over 30°W westward in winter (Figure 7b), PARASOL AOD_c achieves to cross the Atlantic Ocean (60°W) in spring and summer (Figure 7f,i). The much more important transport of coarse mode aerosols as observed through PARASOL AOD_c product is a significant result verified in previous studies [10,30,36,40,92,107,108]. This should be correlated with

the fact that a high contribution of the coarse mode relative to the total AOD was observed over the whole area, as mentioned earlier in the paper. The transport of coarse aerosols over long distances could be explained by the greater number of emissions sources of large aerosols, which statistically increase the probability of coarse mode aerosols reaching the West zone. Apart from Africa, Figure 7 presents a much smaller source of aerosols in the north of Brazil (0°N ; 50°W) (Figure 7, left column) which exhibits the occurrence of coarse mode aerosols only (Figure 7, right column). Because of their limited transport in this West sub-region, coarse mode aerosols emitted from Brazil have a negligible impact on high values of AOD_c found in the East and Centre zones (Figure 7c,f,i,l).

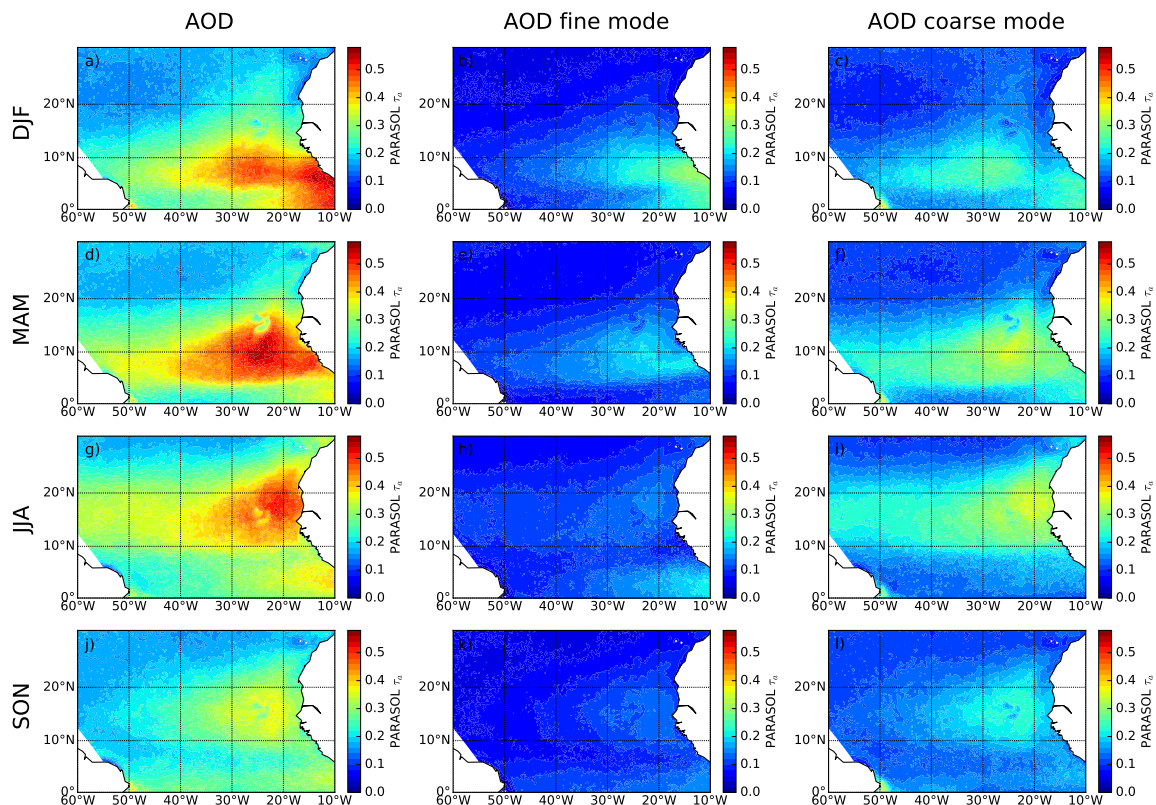


Figure 7. Spatial distribution of PARASOL AOD seasonal mean (2005–2013) at 550 nm: (a–c) winter mean (DJF), (d–f) spring mean (MAM), (g–i) summer mean (JJA) and (j–l) autumn mean (SON). The left column presents total AOD, the center column presents AOD_f and the right column presents AOD_c .

Aerosol coarse and fine modes vary depending on the sub-region and on the season. To study this spatio-temporal variability, Figure 8 presents the interannual variability of PARASOL AOD, AOD_f and AOD_c monthly means for each sub-region (East zone, Centre zone and West zone). Even though AOD_c has the largest impact on AOD over the whole study area, it can be equalized or surpassed by AOD_f at the end of every year in the East zone (Figure 8a), due to the large amount of emitted biomass burning aerosols from the Gulf of Guinea during the dry season. In the Center zone, and even more in the West zone, the influence of AOD_c on AOD is emphasized by the weak transport of PARASOL AOD_f , which is illustrated by the gap between AOD_c and AOD (Figure 8b,c). Thus, cases where AOD_f contribution reaches AOD_c values occur nine times in the East zone, two times in November 2006 and July 2011 in the Center zone (Figure 8b) and no longer occur in the West zone (Figure 8c).

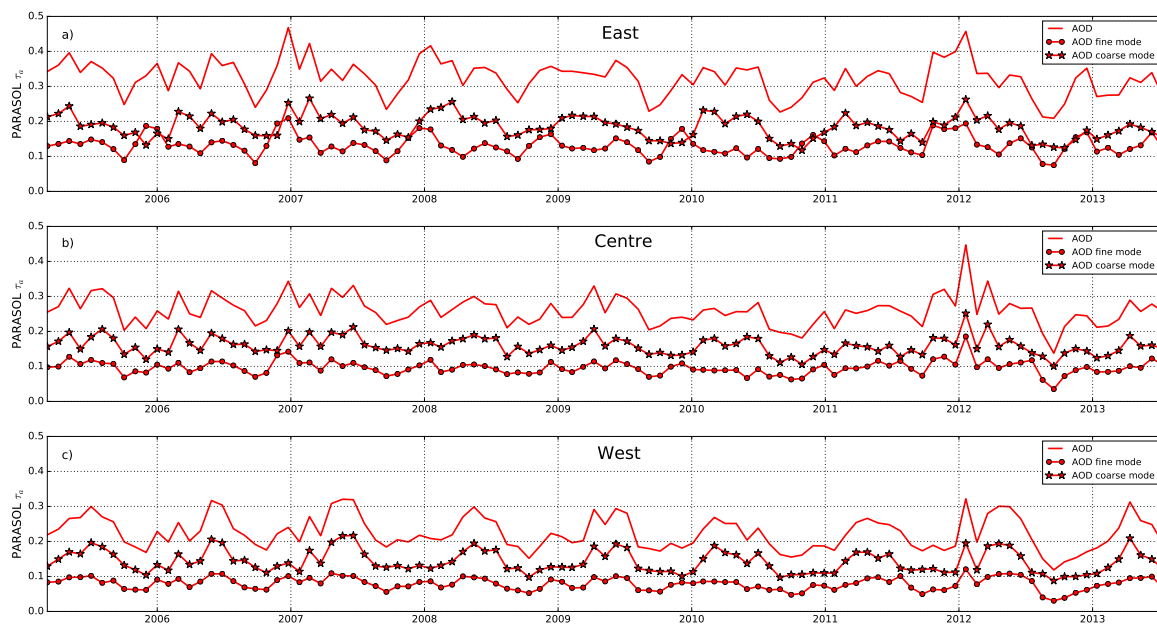


Figure 8. Monthly mean of PARASOL AOD (solid curve), PARASOL AOD_f (line-dots) and PARASOL AOD_c (line-stars) at 550 nm in (a) East zone, (b) Centre zone and (c) West zone. All plots are averaged from 2005 to 2013.

4. Implications for Models Simulations

The previous observations of the aerosol transport, and more specifically the aerosol coarse mode transport, across the NTA ocean is now analysed using reliable reanalysis retrievals that combine modelling and assimilation of AOD observations: MERRA-2 and MACC reanalysis. According to Bellouin et al. [109] and Randles et al. [82], the uncertainties of MACC and MERRA-2 reanalyses are close to 0.03 and 0.013 respectively for the total AOD. The uncertainties are close to 0.014 and 0.010 for MACC and MERRA-2 respectively when dealing with dust AOD_f at 550 nm. Results presented below are calculated only based on coincident PARASOL/MACC/MERRA-2 observations.

Figure 9 presents the spatial distributions of AOD, AOD_f and AOD_c derived from PARASOL (Figure 9a–c) and from MERRA-2 reanalysis (Figure 9d–f). The averaged AOD from 2005 to 2013 as derived from MACC reanalysis is also reported (Figure 9g). In parallel with Figure 9, Table 3 compiles seasonal and annual averages by sub-regions (East, Center and West) of the three AOD products (total, fine, coarse) from PARASOL, MERRA-2 and MACC.

The comparison with MERRA-2 reanalysis shows a significant difference with PARASOL observations: smaller amounts of aerosols are provided by MERRA-2 over the whole domain (Figure 9a,d, Table 3). Such a result could be due to several factors. First, MERRA-2 presents a lower average content of aerosols over the East zone (0.26 for MERRA-2 against 0.33 for PARASOL, Table 3) which may be due in part to an underestimation of winter fine mode aerosol production, i.e dust fine mode fraction and biomass burning aerosol under 10°N (Figure 9e) (winter MERRA-2 AOD_f: 0.10, winter PARASOL AOD_f: 0.16, Table 3). Second, Figure 9d presents a much stronger AOD longitudinal gradient with a faster decrease in the MERRA-2 AOD value from East to West, compared to PARASOL (Figure 9a), thus highlighting a considerably more limited MERRA-2 transport. Indeed, the underestimation of MERRA-2 aerosol content in the East zone cannot entirely be the cause of the low MERRA-2 AOD values found further west since MERRA-2 AOD negative bias, in regard to PARASOL AOD, increases with the distance from african sources (−0.07 in the East zone; −0.09 beyond 30°W). Note that when MERRA-2 dust content is higher than PARASOL content (in summer), MERRA-2 transport of dust remains smaller. A highly underestimated MERRA-2 coarse mode transport, observed in Figure 9f, could explain the origin of this limited transport of aerosol.

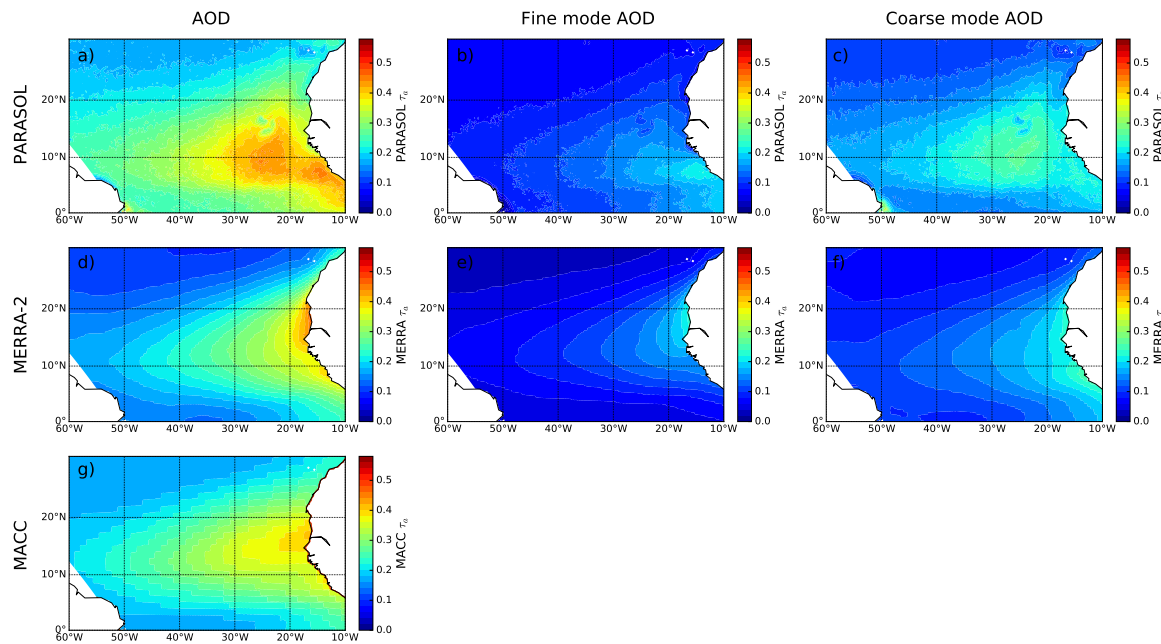


Figure 9. Spatial distribution of mean total AOD total (left column), mean AOD_f (central column) and mean AOD_c (right column) from (a–c) PARASOL satellite, (d–f) MERRA reanalysis and (g) MACC reanalysis averaged from 2005 to 2013.

In parallel, it should be highlighted that since MODIS AOD observations have been assimilated in MERRA-2 reanalysis, a meridional shift of the MERRA-2 maxima of total AOD, AOD_f, and to a lesser extent AOD_c, is expectedly observed in comparison with PARASOL AOD products. However, it is worth noting that MERRA-2 underestimates the aerosol fine mode fraction under 10°N (Figure 9e) whereas MODIS sensor could observe it (Figure 6e). As for the coarse mode, the limited transport of MERRA-2 AOD_c (Figure 9f) may be partly explained by the weaker AOD_c transport in MODIS observations as that observed with PARASOL (Figure 6c,f). However, MERRA-2 process of data assimilation could also potentially be involved, owing to MERRA-2 AOD_c bias with MODIS AOD_c (Table 3).

Compared to MERRA-2, MACC reanalysis presents a transport of aerosols across the ocean (Figure 9g) closer to the one observed in PARASOL (Figure 9a). This is illustrated by a constant bias around $-0.4/-0.3$ in each zone in regard to PARASOL AOD (Table 3). Such better performance occurs despite MACC lower aerosol activity in the East zone where a weaker amount of dust (Figure 9g) is observed, compared to MERRA-2 and PARASOL (Figure 9a,d). Although MACC and MERRA-2 reanalysis differ on several aspects, such as the dust retrieval or the aerosol transport across the ocean, they converge on the estimated content of aerosol coming from equatorial Africa. However, with weaker values than those observed by PARASOL and MODIS, the estimated production may be underestimated. MACC reanalysis also provides the advantage of distinguishing between different types of aerosols (mineral dust, anthropogenic aerosol and sea salt aerosol) whose spatial distributions are shown in Figure 10. These simulations indicate that, even if sea salt AOD has generally much lower values compared to dust (ranging from 0.10 to 0.20) (Figure 10c), AOD reaches the value 0.10 in the central part of the Atlantic (Figure 10d) thus highlighting the non-negligible role of sea salt aerosols in this area in terms of contribution to the total extinction (Figure 10a). The contribution of anthropogenic aerosols, notably biomass burning aerosols, is limited to a more restricted area that is located close to the source of aerosol production (Figure 10b). The simulated limited transport of fine mode aerosols strengthens the assumption previously made by Adams et al. [110]. Our results confirm the important role of dust coarse aerosols in the field of aerosols transport study.

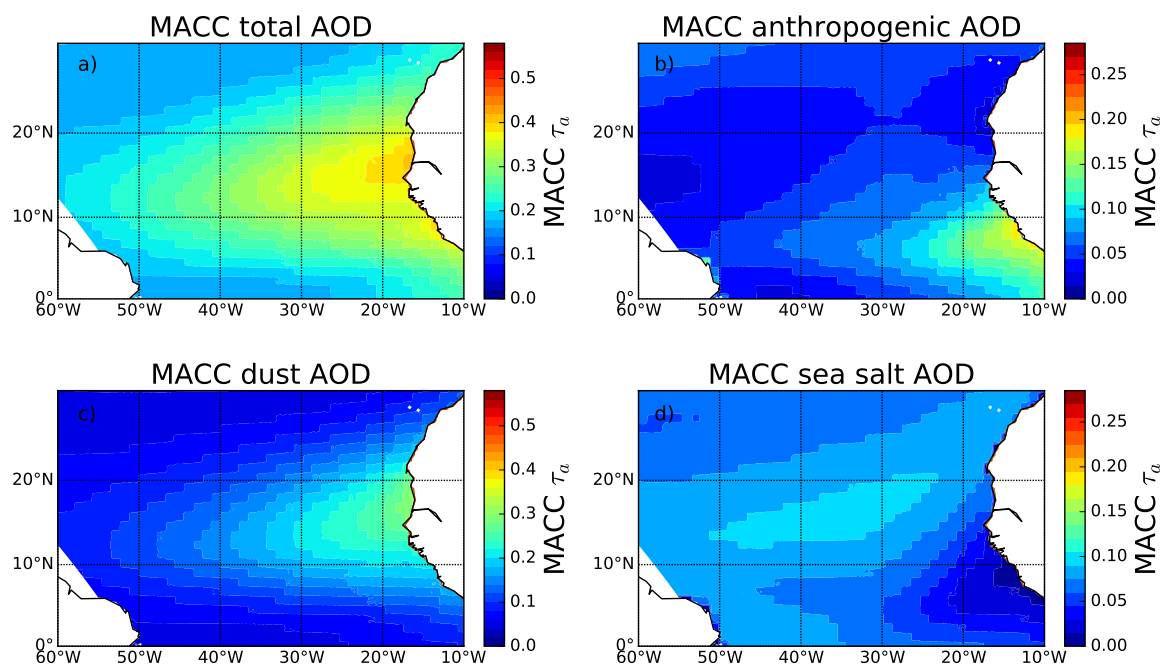


Figure 10. Spatial distribution of (a) total AOD total, (b) anthropogenic AOD, (c) dust AOD and (d) sea salt AOD from MACC reanalysis at 550 nm averaged from 2005 to 2013.

In summary, the comparison of the aerosol transport between PARASOL and model reanalysis outputs revealed that models tend to underestimate the aerosol transport over the NTA ocean, which is probably due to an underestimation of the coarse mode transport of aerosols.

5. Discussion

Over the NTA ocean, the quarterly variations of a long time series of satellite observations obtained by PARASOL processed using the new POLAC atmospheric correction algorithm provide a satisfactory overview of the seasonal variability of aerosols, allowing the distinction between total, fine and coarse mode aerosols. Driven by the seasonal shift of the ITCZ and its impact on the SAL export [111], the aerosol seasonal variability is mainly induced by mineral dust advection over the ocean as shown by the large contribution of PARASOL AOD_c relative to the total AOD and by their location over $10^\circ N$. The high concentration of coarse mode aerosols close to the source of production and its decrease during transatlantic transport to the Caribbean are well observed by PARASOL. It strengthens the result obtained from previous works related to dust transport (e.g., [23–25,92]); some of which use other satellite sensors like MODIS and IASI [8,41,112]. Based on the performance of POLAC/PARASOL observations of AOD and AOD_c assessed through a comparison with ground-based AERONET measurements, this study thereby confirms the enhanced long-range transport of coarse particles, such as mineral dust, over our study area.

Note that the coexistence of mineral dust and clouds could exist. However, since our satellite and AERONET data were analysed for cloud-free conditions only, it is not possible in this study to examine the consequences of such a coexistence on the comparison between observations and models. This is one limitation of our approach.

5.1. Comparison with Previous Experimental Campaigns and Satellite Data

Several field campaigns have been realized on dust aerosol transport across the Atlantic Ocean to the Caribbean. Under the Saharan Aerosol Long-Range Transport and Aerosol-Cloud-Interaction Experiment (SALTRACE) project, ground-based and airborne in situ remote sensing observations in Barbados, Puerto Rico and Cabo Verde were conducted from spring 2013 to summer 2014 [92].

Weinzierl et al. [92] exhibit the major contribution of dust to the AOD in the Caribbean and detect the unexpected presence of 10–30 μm particles even after 5 days of transport and more than 4000 km. Based on Denjean et al. [113] showing that modal peak diameter of the volume size distribution remained constant on both sides of the Atlantic, Weinzierl et al. [92] suggest that after 2–3 days from uplift gravitational settling is almost ineffective. These conclusions are consistent with Maring et al. [30] who, from comparisons between surface based measurements at sites in the Canary islands (July 1995) and in Puerto Rico (July 2000), conclude that some atmospheric processes partially counteract gravitational settling of large dust particles. Velasco-Merino et al. [107] also evaluated the impact of the transport over the Atlantic Ocean on Saharan dust optical and microphysical properties based on AERONET data. They show a decrease of about 30% in the coarse-mode concentration of the size distributions but no significant change in the coarse-mode effective radius during the transport. All these studies present total AOD values similar to our results with maximum peaks reaching 0.6 in summer near the west coast of Africa and around 0.3 in the Caribbean.

To characterize aerosol transport over the Atlantic Ocean, several other studies rely on satellite sensors and their inherent advantages over ground-based measurements due to their spatial and temporal coverage. Among them, Kalashnikova and Kahn [36], Yu et al. [35] and Prospero et al. [10] have described the significant dust transport across the tropical North Atlantic over the course of one year. They all show consistent seasonal variations of trans-Atlantic dust transport but present notable differences in the magnitude of dust AOD, with PARASOL dust transport higher than MODIS and much higher than MISR [35]. Our study stands apart by distinguishing the fine mode of AOD, which may include the contribution of several types of aerosols, from the coarse mode of AOD, which is likely dominated by dust [16,17]. It should be mentioned that those previous studies also did not perform such an extensive evaluation as the one presented in this paper since their investigations did not concern such a long period of time series or such a large spatial extent.

5.2. Possible Causes of the Long-Range Transport of Coarse Mode Aerosols

One of the most important factors that determine the transport of coarse mode aerosols is the vertical distribution (e.g., [114]). During summer, coarse mode aerosol transport across the Atlantic Ocean mainly occurs in the SAL. As shown by CALIOP [34,103,110,114,115], the SAL is located above the top of the marine boundary layer and typically 3–4 km high. Thus, the transport of the coarse mode could cover great distances. This transatlantic transport ends in the Caribbean where aerosols are transferred from the SAL to the marine boundary layer, by gravitational settling of mainly coarse mode particles and through convective and turbulent downward mixing [92]. This makes it different from, for example, fine biomass burning aerosols which are less influenced by the trade wind since the latter restricts their transport [116] over the ocean. The seasonal meteorological regime may explain the long-distance transport of the coarse mode aerosol by causing the elevation of the dust layers over the West Africa at higher levels during summer than during winter [117]. Indeed, while long-range dust transport occurs in summer at high altitude within the SAL above the trade winds inversion (~1.5 km above sea level), the winter time long-range dust transport takes place in a low layer within the trade winds [118]. However, Figure 7c shows that coarse mode aerosol transport exceeds the fine mode aerosol transport even during winter. Such differences in long-distance transport must be correlated to aerosol fine mode or coarse mode attribution.

5.3. Long-Range Transport of Coarse Mode Aerosols in Reanalysis

Our study also highlights the difficulty for model reanalysis to properly estimate the aerosol optical depth over the study area, despite the use of data assimilation. Kim et al. [115] reached a similar conclusion by presenting a multimodel analysis and comparison with remote sensing data. Contrary to satellites which show general agreement, Kim et al. [115] revealed that models display considerable discrepancy with each other, with significant differences between the models and observation as well as among the models. In our study, such discrepancy is illustrated by an underestimation of the aerosol

transport over the ocean, more or less important regarding the type of model reanalysis (MACC or MERRA-2). Even though MACC AOD values are slightly lower than observations, MACC reanalysis shows a satisfactory transport of aerosols over the NTA ocean (Figure 9g) while it is not the case for MERRA-2 reanalysis. It seems that the inability of MERRA-2 to reproduce a long distance transport as high as measured by POLDER/PARASOL comes from a significant underestimation of the coarse mode aerosol transport over the ocean (Figure 9f). The underestimation occurs despite the fact that assimilation of accurate MODIS observations, of both AOD and AOD_c, are performed in MERRA-2 reanalysis (Figure 6d). It might suggest a weakness either in MERRA-2 process of data assimilation or in MERRA-2 wet and dry deposition parameterization. Such a deficiency in the evaluation of coarse mode particles along the trans-Atlantic transect has already been highlighted by Ansmann et al. [119] and Kok [120] in climate models. According to Ansmann et al. [119] based on SALTRACE campaign observations, an important removal of dust is observed in a regional model (SKIRON) and two global atmospheric models (MACC/CAMS, NMMB/BSC-Dust), as in Weinzierl et al. [92], where the main process of vertical exchange in the well-stratified SAL relies on particle settling through sedimentation. Gravitational settling depending on the simulated fine and coarse dust fractions [119], this result is coherent with Kok [120]. Indeed, the latter shows an underestimation of the coarse size fraction in climate models which may result from the sampling of dust specific size classes (PM₁₀, PM_{2.5}), as it is performed in MERRA-2. However, these possible causes cannot be the only explanations of the underestimation of the coarse mode particles along the trans-Atlantic transect in models. Mechanisms than retain these particles in the atmosphere during long-range transport must be involved [119].

The higher performance of MACC reanalysis, relatively to MERRA-2, for deriving the AOD is consistent with recent studies [82,83]. Randles et al. [83] suggested that MERRA-2 absorption is overestimated in areas far from aerosol sources (e.g the free troposphere) because of excessive amounts of black carbon aerosol and because the probability of precipitation of aerosols that reach the free atmosphere is almost null.

Yet, it is crucial to accurately assimilate the coarse mode of aerosols in models reanalysis. Aerosols with diameters around 0.05–10 μm are of great interest because of their direct interaction with solar and infrared radiation. Their overestimation or underestimation in climate models can likely be the causes of errors in the magnitude, and possibly, the sign of the modeled aerosol radiative forcing, depending on local parameters such as the surface albedo. A wrong consideration of aerosol coarse mode could result in erroneous numerical weather forecasting and regional climate predictions in areas which are affected by aerosol emission or transport. As an example, the consequences resulting from errors in the estimation of the coarse/fine mode of aerosols may lead to:

- a possible error on the radiative forcing exerted by dust aerosols at the top of the atmosphere in case of erroneous retrievals of fine mode aerosols: less fine aerosols could lead to less radiative cooling;
- a possible underestimation of warming at the top of the atmosphere in the longwave spectral range since more coarse dust aerosols lead to a higher warming;
- a possible important change in the ability of dust (aged) aerosols to act as aerosol-cloud condensation nuclei.

6. Conclusions

The POLDER/PARASOL ability to measure the polarization state of light was exploited here to analyze a time series (from 2005 to 2013) of the amount of fine and coarse modes aerosols over the NTA ocean using a dedicated algorithm, namely the POLAC. In addition to the consistency between PARASOL data and MODIS observations, it was shown that POLAC/PARASOL products satisfactorily compared with AERONET ground-based measurements, with correlation coefficients over 0.75 and bias ranging from -0.03 and 0.03 for PARASOL AOD and PARASOL AOD_c products respectively. Daily PARASOL aerosol products were then used to analyse the spatio-temporal variability of the total, fine mode and coarse mode aerosols. It clearly underlined a significant contribution of the dust coarse mode relative to the total AOD (from 15% to 65%) over the whole study area, which is

consistent with previous studies using in situ observations from experimental campaigns or satellite data. Such significant transport of coarse dust mode aerosols observed by PARASOL and MODIS dataset is not reproduced by MERRA-2 reanalysis which showed a negative bias (around -0.06 beyond 30°W). At this stage, it is difficult to identify the possible causes in the differences observed in the dust coarse mode between PARASOL and MERRA-2 reanalysis. However, as described recently by Weinzierl et al. [92] and Ansmann et al. [119] using SALTRACE observations, the daytime convective mixing within the SAL would allow a significant fraction of coarse mode aerosols to reach the Caribbean by balancing the sedimentation. Then, one reason could be related to a deficient reproduction of the dynamics in the SAL layer in models. Our study also confirms that satellite polarimetric and multidirectional daily observations, such as the POLDER/PARASOL sensor or the forthcoming “Multi-viewing Multi-channel Multi-polarization Imaging (3MI)” sensor (ESA/EUMETSAT) and the PACE sensor (NASA), should be helpful for providing additional constraints to evaluate the representation of fine/coarse dust aerosols in global and regional models.

Author Contributions: Conceptualization, M.C. and M.M.; methodology, M.C. and M.M.; validation, H.F., M.C. and M.M.; formal analysis, H.F., M.C. and M.M.; investigation, H.F., M.C. and M.M.; writing—original draft preparation, H.F.; writing—review and editing, H.F., M.C. and M.M.; supervision, M.C. and M.M.; project administration, M.C.; funding acquisition, M.C. and M.M. All authors have read and agreed to the published version of the manuscript.

Funding: This research was funded by the Centre National d'Études Spatiales (CNES-France) throughout the project “POLDUST” and the grant of Hélène Fréville.

Acknowledgments: We would like to thank the ‘Pôle de données et de services AERIS-ICARE’ (CNES/CNRS-INSU) for the distribution of POLAC/PARASOL data (<http://www.icare.univ-lille1.fr>). We are grateful to NASA (USA) for distributing the MODIS (<https://modis-atmos.gsfc.nasa.gov/products/monthly>), MERRA-2 (<https://gmao.gsfc.nasa.gov/reanalysis/MERRA-2>) and AERONET (<https://aeronet.gsfc.nasa.gov>) data. We would like to thank each AERONET Principal Investigators, namely Detlef Stammer, Emilio Cuevas-Agullo, Francisco Javier Expósito Gonzales, Joseph Prospero and their staff for establishing and maintaining the AERONET sites that were used in this study. We also would like to thank the European Center for Medium-Range Weather Forecasts (ECMWF) for the distribution of MACC reanalysis (apps.ecmwf.int/datasets/data/macc-reanalysis). We would like to thank Tristan Harmel and Bernard Gentili for helpful discussions.

Conflicts of Interest: The authors declare no conflict of interest.

Abbreviations

The following abbreviations are used in this manuscript:

AOD Aerosol optical depth
NTA North Tropical Atlantic

References

1. Evan, A.T.; Heidinger, A.K.; Bennartz, R.; Bennington, V.; Mahowald, N.M.; Corrada-Bravo, H.; Velden, C.S.; Myhre, G.; Kossin, J.P. Ocean temperature forcing by aerosols across the atlantic tropical cyclone development region. *Geochem. Geophys. Geosyst.* **2008**, *9*, doi:10.1029/2007GC001774. [[CrossRef](#)]
2. Forster, P.; Ramaswamy, V.; Artaxo, P.; Berntsen, T.; Betts, R.; Fahey, D.W.; Haywood, J.; Lean, J.; Lowe, D.C.; Myhre, G.; et al. Changes in atmospheric constituents and in radiative forcing. In *Climate Change 2007. The Physical Science Basis*; Chapter 2; Cambridge University Press: Cambridge, UK, 2007.
3. Haywood, J.; Francis, P.; Osborne, S.; Glew, M.; Loeb, N.; Highwood, E.; Tanré, D.; Myhre, G.; Formenti, P.; Hirst, E. Radiative properties and direct radiative effect of saharan dust measured by the c-130 aircraft during shade: 1. Solar spectrum. *J. Geophys. Res. Atmos.* **2003**, *108*, doi:10.1029/2002JD002687. [[CrossRef](#)]
4. Kim, K.-M.; Lau, W.K.-M.; Sud, Y.C.; Walker, G.K. Influence of aerosol-radiative forcings on the diurnal and seasonal cycles of rainfall over west africa and eastern atlantic ocean using gcm simulations. *Clim. Dyn.* **2010**, *35*, 115–126. [[CrossRef](#)]
5. Zhao, C.; Liu, X.; Leung, L.; Johnson, B.; McFarlane, S.A.; Gustafson, W., Jr.; Fast, J.D.; Easter, R. The spatial distribution of mineral dust and its shortwave radiative forcing over north africa: Modeling sensitivities to dust emissions and aerosol size treatments. *Atmos. Chem. Phys.* **2010**, *10*, 8821–8838. [[CrossRef](#)]

6. Jickells, T.; An, Z.; Andersen, K.K.; Baker, A.; Bergametti, G.; Brooks, N.; Cao, J.; Boyd, P.; Duce, R.; Hunter, K.; et al. Global iron connections between desert dust, ocean biogeochemistry, and climate. *Science* **2005**, *308*, 67–71. [[CrossRef](#)]
7. Maher, B.; Prospero, J.; Mackie, D.; Gaiero, D.; Hesse, P.P.; Balkanski, Y. Global connections between aeolian dust, climate and ocean biogeochemistry at the present day and at the last glacial maximum. *Earth Sci. Rev.* **2010**, *99*, 61–97. [[CrossRef](#)]
8. Kaufman, Y.; Koren, I.; Remer, L.; Tanré, D.; Ginoux, P.; Fan, S. Dust transport and deposition observed from the terra-moderate resolution imaging spectroradiometer (modis) spacecraft over the atlantic ocean. *J. Geophys. Res. Atmos.* **2005**, *110*, doi:10.1029/2003JD004436. [[CrossRef](#)]
9. Kaufman, Y.J.; Tanré, D.; Boucher, O. A satellite view of aerosols in the climate system. *Nature* **2002**, *419*, 215. [[CrossRef](#)]
10. Prospero, J.M.; Collard, F.-X.; Molinié, J.; Jeannot, A. Characterizing the annual cycle of african dust transport to the caribbean basin and south america and its impact on the environment and air quality. *Glob. Biogeochem. Cycles* **2014**, *28*, 757–773. [[CrossRef](#)]
11. Bernstein, L.; Bosch, P.; Canziani, O.; Chen, Z.; Christ, R.; Riahi, K. *IPCC, 2007: Climate Change 2007: Synthesis Report*; IPCC: Geneva, Switzerland, 2008.
12. Bond, T.C.; Doherty, S.J.; Fahey, D.; Forster, P.; Berntsen, T.; DeAngelo, B.; Flanner, M.; Ghan, S.; Kärcher, B.; Koch, D.; et al. Bounding the role of black carbon in the climate system: A scientific assessment. *J. Geophys. Res. Atmos.* **2013**, *118*, 5380–5552. [[CrossRef](#)]
13. Charlson, R.J.; Schwartz, S.; Hales, J.; Cess, R.D.; Coakley, J.J.; Hansen, J.; Hofmann, D. Climate forcing by anthropogenic aerosols. *Science* **1992**, *255*, 423–430. [[CrossRef](#)]
14. Haywood, J.; Boucher, O. Estimates of the direct and indirect radiative forcing due to tropospheric aerosols: A review. *Rev. Geophys.* **2000**, *38*, 513–543. [[CrossRef](#)]
15. Tegen, I.; Hollrig, P.; Chin, M.; Fung, I.; Jacob, D.; Penner, J. Contribution of different aerosol species to the global aerosol extinction optical thickness: Estimates from model results. *J. Geophys. Res. Atmos.* **1997**, *102*, 23895–23915. [[CrossRef](#)]
16. Huneus, N.; Schulz, M.; Balkanski, Y.; Griesfeller, J.; Prospero, M.; Kinne, S.; Bauer, S.; Boucher, O.; Chin, M.; Dentener, F.; et al. Global dust model intercomparison in aerocom phase i. *Atmos. Chem. Phys.* **2011**, *11*, 7781–7816.
17. Kinne, S.; Schulz, M.; Textor, C.; Guibert, S.; Balkanski, Y.; Bauer, S.; Berntsen, T.; Berglen, T.; Boucher, O.; Chin, M.; et al. An aerocom initial assessment—Optical properties in aerosol component modules of global models. *Atmos. Chem. Phys. Discuss.* **2005**, *5*, 8285–8330. [[CrossRef](#)]
18. Prospero, J.M.; Ginoux, P.; Torres, O.; Nicholson, S.E.; Gill, T.E. Environmental characterization of global sources of atmospheric soil dust identified with the nimbus 7 total ozone mapping spectrometer (toms) absorbing aerosol product. *Rev. Geophys.* **2002**, *40*, doi:10.1029/2000RG000095. [[CrossRef](#)]
19. Schepanski, K.; Heinold, B.; Tegen, I. Harmattan, saharan heat low, and west african monsoon circulation: Modulations on the saharan dust outflow towards the north atlantic. *Atmos. Chem. Phys.* **2017**, *17*, 10223. [[CrossRef](#)]
20. Diaz, H.F.; Carlson, T.N.; Prospero, J.M. *A study of the Structure and Dynamics of the Saharan Air Layer over the Northern Equatorial Atlantic during BOMEX*; NOAA Technical Memorandum, ERL WMPO-32; Environmental Research Laboratories (U.S.). Weather Modification Program Office. National Hurricane and Experimental Meteorology Laboratory: Virginia Key, FL, USA, 1976; 61 p.
21. Dunion, J.P.; Velden, C.S. The impact of the saharan air layer on atlantic tropical cyclone activity. *Bull. Am. Meteorol. Soc.* **2004**, *85*, 353–365. [[CrossRef](#)]
22. Prospero, J.M.; Carlson, T.N. Vertical and areal distribution of saharan dust over the western equatorial north atlantic ocean. *J. Geophys. Res.* **1972**, *77*, 5255–5265. [[CrossRef](#)]
23. Prospero, J.M.; Lamb, P.J. African droughts and dust transport to the caribbean: Climate change implications. *Science* **2003**, *302*, 1024–1027. [[CrossRef](#)]
24. Stevens, B.; Farrell, D.; Hirsch, L.; Jansen, F.; Nuijens, L.; Serikov, I.; Brüggemann, B.; Forde, M.; Linne, H.; Lonitz, K.; et al. The barbados cloud observatory: Anchoring investigations of clouds and circulation on the edge of the itcz. *Bull. Am. Meteorol. Soc.* **2016**, *97*, 787–801. [[CrossRef](#)]
25. Prospero, J.M. Long-range transport of mineral dust in the global atmosphere: Impact of african dust on the environment of the southeastern united states. *Proc. Natl. Acad. Sci. USA* **1999**, *96*, 3396–3403. [[CrossRef](#)]

26. Swap, R.; Garstang, M.; Greco, S.; Talbot, R.; Källberg, P. Saharan dust in the amazon basin. *Tellus B* **1992**, *44*, 133–149. [[CrossRef](#)]
27. Ansmann, A.; Baars, H.; Tesche, M.; Müller, D.; Althausen, D.; Engelmann, R.; Pauliquevis, T.; Artaxo, P. Dust and smoke transport from africa to south america: Lidar profiling over cape verde and the amazon rainforest. *Geophys. Res. Lett.* **2009**, *36*, doi:10.1029/2009GL037923. [[CrossRef](#)]
28. Chouza, F.; Reitebuch, O.; Benedetti, A.; Weinzierl, B. Saharan dust long-range transport across the atlantic studied by an airborne doppler wind lidar and the macc model. *Atmos. Chem. Phys.* **2016**, *16*, 11581–11600. [[CrossRef](#)]
29. García, M.I.; Rodríguez, S.; Alastuey, A. Impact of north america on the aerosol composition in the north atlantic free troposphere. *Atmos. Chem. Phys.* **2017**, *17*, 7387. [[CrossRef](#)]
30. Maring, H.; Savoie, D.; Izaguirre, M.; Custals, L.; Reid, J. Mineral dust aerosol size distribution change during atmospheric transport. *J. Geophys. Res. Atmos.* **2003**, *108*, doi:10.1029/2002JD002536. [[CrossRef](#)]
31. Martet, M.; Peuch, V.; Laurent, B.; Marticorena, B.; Bergametti, G. Evaluation of long-range transport and deposition of desert dust with the ctm mocage. *Tellus B Chem. Phys. Meteorol.* **2009**, *61*, 449–463. [[CrossRef](#)]
32. Rodríguez, S.; Cuevas, E.; Prospero, J.; Alastuey, A.; Querol, X.; López-Solano, J.; García, M.; Alonso-Pérez, S. Modulation of saharan dust export by the north african dipole. *Atmos. Chem. Phys.* **2015**, *15*, 7471–7486. [[CrossRef](#)]
33. Rodríguez González, S.; Alastuey, A.; Alonso-Pérez, S.; Querol, X.; Agulló, E.C.; Afonso, J.A.; Viana, M.; Pérez, N.; Pandolfi, M.; Rosa, J.D.D.L. Transport of desert dust mixed with north african industrial pollutants in the subtropical saharan air layer. *Atmos. Chem. Phys.* **2011**, *11*, doi:10.5194/acp-11-6663-2011. [[CrossRef](#)]
34. Tsamalis, C.; Chédin, A.; Pelon, J.; Capelle, V. The seasonal vertical distribution of the saharan air layer and its modulation by the wind. *Atmos. Chem. Phys.* **2013**, *13*, 11235–11257. [[CrossRef](#)]
35. Yu, H.; Remer, L.A.; Chin, M.; Bian, H.; Tan, Q.; Yuan, T.; Zhang, Y. Aerosols from overseas rival domestic emissions over north america. *Science* **2012**, *337*, 566–569. [[CrossRef](#)]
36. Kalashnikova, O.V.; Kahn, R.A. Mineral dust plume evolution over the atlantic from misr and modis aerosol retrievals. *J. Geophys. Res. Atmos.* **2008**, *113*, doi:10.1029/2008JD010083. [[CrossRef](#)]
37. Chiapello, I.; Moulin, C.; Prospero, J.M. Understanding the long-term variability of african dust transport across the atlantic as recorded in both barbados surface concentrations and large-scale total ozone mapping spectrometer (toms) optical thickness. *J. Geophys. Res. Atmos.* **2005**, *110*, doi:10.1029/2004JD005132. [[CrossRef](#)]
38. Heintzenberg, J.; Charlson, R.; Clarke, A.; Lioussé, C.; Ramaswamy, V.; Shine, K.; Wendisch, M.; Helas, G. Measurements and modelling of aerosol single-scattering albedo: Progress, problems and prospects. *Contrib. Atmos. Phys.* **1997**, *70*, 249–263.
39. Sokolik, I.; Toon, O. Direct radiative forcing by airborne mineral aerosols. *J. Aerosol Sci.* **1996**, *27*, S11–S12. [[CrossRef](#)]
40. Yu, H.; Remer, L.A.; Kahn, R.A.; Chin, M.; Zhang, Y. Satellite perspective of aerosol intercontinental transport: From qualitative tracking to quantitative characterization. *Atmos. Res.* **2013**, *124*, 73–100. [[CrossRef](#)]
41. Bréon, F.-M.; Vermeulen, A.; Descloitres, J. An evaluation of satellite aerosol products against sunphotometer measurements. *Remote Sens. Environ.* **2011**, *115*, 3102–3111. [[CrossRef](#)]
42. Dubovik, O.; Herman, M.; Holdak, A.; Lapyonok, T.; Tanré, D.; Deuzé, J.; Ducos, F.; Sinyuk, A.; Lopatin, A. Statistically optimized inversion algorithm for enhanced retrieval of aerosol properties from spectral multi-angle polarimetric satellite observations. *Atmos. Meas. Tech.* **2011**, *4*, 975. [[CrossRef](#)]
43. Harmel, T.; Chami, M. Influence of polarimetric satellite data measured in the visible region on aerosol detection and on the performance of atmospheric correction procedure over open ocean waters. *Opt. Express* **2011**, *19*, 20960–20983. [[CrossRef](#)]
44. Levy, R.C.; Remer, L.A.; Mattoo, S.; Vermote, E.F.; Kaufman, Y.J. Second-generation operational algorithm: Retrieval of aerosol properties over land from inversion of moderate resolution imaging spectroradiometer spectral reflectance. *J. Geophys. Res. Atmos.* **2007**, *112*, doi:10.1029/2006JD007811. [[CrossRef](#)]
45. Tanré, D. Derivation of tropospheric aerosol properties from satellite observations. *Comptes Rendus Geosci.* **2010**, *342*, 403–411. [[CrossRef](#)]
46. Tanré, D.; Bréon, F.; Deuzé, J.; Dubovik, O.; Ducos, F.; François, P.; Goloub, P.; Herman, M.; Lifermann, A.; Waquet, F. Remote sensing of aerosols by using polarized, directional and spectral measurements within the a-train: The parasol mission. *Atmos. Meas. Tech.* **2011**, *4*, 1383–1395. [[CrossRef](#)]

47. Veselovskii, I.; Kolgotin, A.; Griaznov, V.; Müller, D.; Franke, K.; Whiteman, D.N. Inversion of multiwavelength raman lidar data for retrieval of bimodal aerosol size distribution. *Appl. Opt.* **2004**, *43*, 1180–1195. [[CrossRef](#)]
48. Wang, Y.; Fan, S.; Feng, X.; Yan, G.; Guan, Y. Regularized inversion method for retrieval of aerosol particle size distribution function in w 1, 2 space. *Appl. Opt.* **2006**, *45*, 7456–7467. [[CrossRef](#)]
49. Mishchenko, M.I.; Travis, L.D. Satellite retrieval of aerosol properties over the ocean using polarization as well as intensity of reflected sunlight. *J. Geophys. Res. Atmos.* **1997**, *102*, 16989–17013. [[CrossRef](#)]
50. Chami, M. Importance of the polarization in the retrieval of oceanic constituents from the remote sensing reflectance. *J. Geophys. Res. Oceans* **2007**, *112*, doi:10.1029/2006JC003843. [[CrossRef](#)]
51. Chowdhary, J.; Cairns, B.; Travis, L.D. Case studies of aerosol retrievals over the ocean from multiangle, multispectral photopolarimetric remote sensing data. *J. Atmos. Sci.* **2002**, *59*, 383–397. [[CrossRef](#)]
52. Harmel, T.; Chami, M. Invariance of polarized reflectance measured at the top of atmosphere by parasol satellite instrument in the visible range with marine constituents in open ocean waters. *Opt. Express* **2008**, *16*, 6064–6080. [[CrossRef](#)]
53. Inness, A.; Baier, F.; Benedetti, A.; Bouarar, I.; Chabrillat, S.; Clark, H.; Clerbaux, C.; Coheur, P.; Engelen, R.; Errera, Q.; et al. The macc reanalysis: An 8 yr data set of atmospheric composition. *Atmos. Chem. Phys.* **2013**, *13*, 4073–4109. [[CrossRef](#)]
54. Gelaro, R.; McCarty, W.; Suárez, M.J.; Todling, R.; Molod, A.; Takacs, L.; Randles, C.A.; Darmenov, A.; Bosilovich, M.G.; Reichle, R.; et al. The modern-era retrospective analysis for research and applications, version 2 (merra-2). *J. Clim.* **2017**, *30*, 5419–5454. [[CrossRef](#)]
55. Duce, R. Sources, distributions, and fluxes of mineral aerosols and their relation to climate. In *Aerosol Forcing Climate*; Charlson, R.J., Heintzenberg, J., Eds.; John Wiley & Sons Ltd.: Chichester, UK, 1995.
56. Prospero, J. Saharan dust transport over the north atlantic ocean and mediterranean: An overview. In *The Impact of Desert Dust across the Mediterranean*; Springer: Dordrecht, The Netherlands, 1996; pp. 133–151.
57. Prospero, J.M. The atmospheric transport of particles to the ocean. *Scope-Sci. Comm. Probl. Environ. Int. Counc. Sci. Unions* **1996**, *57*, 19–52.
58. Duce, R.; Liss, P.; Merrill, J.; Atlas, E.; Buat-Menard, P.; Hicks, B.; Miller, J.; Prospero, J.; Arimoto, R.; Church, T.; et al. The atmospheric input of trace species to the world ocean. *Glob. Biogeochem. Cycles* **1991**, *5*, 193–259. [[CrossRef](#)]
59. O'Dowd, C.D.; Smith, M.H. Physicochemical properties of aerosols over the northeast atlantic: Evidence for wind-speed-related submicron sea-salt aerosol production. *J. Geophys. Res. Atmos.* **1993**, *98*, 1137–1149. [[CrossRef](#)]
60. Duncan, B.N.; Martin, R.V.; Staudt, A.C.; Yevich, R.; Logan, J.A. Interannual and seasonal variability of biomass burning emissions constrained by satellite observations. *J. Geophys. Res. Atmos.* **2003**, *108*, doi:10.1029/2002JD002378. [[CrossRef](#)]
61. Herman, M.; Deuzé, J.-L.; Marchand, A.; Roger, B.; Lallart, P. Aerosol remote sensing from polder/adeos over the ocean: Improved retrieval using a nonspherical particle model. *J. Geophys. Res. Atmos.* **2005**, *110*, doi:10.1029/2004JD004798. [[CrossRef](#)]
62. Dubovik, O.; Lapyonok, T.; Litvinov, P.; Herman, M.; Fuertes, D.; Ducos, F.; Lopatin, A.; Chaikovskiy, A.; Torres, B.; Derimian, Y.; et al. GRASP: A versatile algorithm for characterizing the atmosphere. *SPIE Newsroom* **2014**, *25*, doi:10.1117/2.1201408.005558. [[CrossRef](#)]
63. Volten, H.; Munoz, O.; Rol, E.; Haan, J.D.; Vassen, W.; Hovenier, J.; Muinonen, K.; Nousiainen, T. Scattering matrices of mineral aerosol particles at 441.6 nm and 632.8 nm. *J. Geophys. Res. Atmos.* **2001**, *106*, 17375–17401. [[CrossRef](#)]
64. Gordon, H.R. Atmospheric correction of ocean color imagery in the earth observing system era. *J. Geophys. Res. Atmos.* **1997**, *102*, 17081–17106. [[CrossRef](#)]
65. Duforêt, L.; Frouin, R.; Dubuisson, P. Importance and estimation of aerosol vertical structure in satellite ocean-color remote sensing. *Appl. Opt.* **2007**, *46*, 1107–1119. [[CrossRef](#)]
66. Harmel, T. Apport des Mesures Directionnelles et Polarisées aux Corrections Atmosphériques Au-Dessus des Océans ouverts: Application à la Mission Parasol. Ph.D. Thesis, Université de Pierre et Marie Curie, Paris, France, 2009.

67. Formenti, P.; Kabuiku, L.M.; Chiapello, I.; Ducos, F.; Dulac, F.; Tanré, D. Aerosol optical properties derived from POLDER-3/PARASOL (2005–2013) over the western Mediterranean Sea: Quality assessment with AERONET and in situ airborne observations. *Atmos. Meas. Tech. Discuss.* **2018**. [[CrossRef](#)]
68. Holben, B.N.; Eck, T.F.; Slutsker, I.; Tanre, D.; Buis, J.; Setzer, A.; Vermote, E.; Reagan, J.; Kaufman, Y.; Nakajima, T.; et al. Aeronet—A federated instrument network and data archive for aerosol characterization. *Remote Sens. Environ.* **1998**, *66*, 1–16.
69. Kleidman, R.G.; O'Neill, N.T.; Remer, L.A.; Kaufman, Y.J.; Eck, T.F.; Tanré, D.; Dubovik, O.; Holben, B.N. Comparison of moderate resolution imaging spectroradiometer (modis) and aerosol robotic network (aeronet) remote-sensing retrievals of aerosol fine mode fraction over ocean. *J. Geophys. Res. Atmos.* **2005**, *110*. [[CrossRef](#)]
70. Dubovik, O.; Holben, B.; Eck, T.F.; Smirnov, A.; Kaufman, Y.J.; King, M.D.; Tanré, D.; Slutsker, I. Variability of absorption and optical properties of key aerosol types observed in worldwide locations. *J. Atmos. Sci.* **2002**, *59*, 590–608. [[CrossRef](#)]
71. O'Neill, N.; Eck, T.; Smirnov, A.; Holben, B.; Thulasiraman, S. Spectral discrimination of coarse and fine mode optical depth. *J. Geophys. Res. Atmos.* **2003**, *108*, doi:10.1029/2002JD002975. [[CrossRef](#)]
72. Eck, T.; Holben, B.; Reid, J.; Dubovik, O.; Smirnov, A.; O'Neill, N.; Slutsker, I.; Kinne, S. Wavelength dependence of the optical depth of biomass burning, urban, and desert dust aerosols. *J. Geophys. Res. Atmos.* **1999**, *104*, 31333–31349. [[CrossRef](#)]
73. Omar, A.; Winker, D.; Tackett, J.; Giles, D.; Kar, J.; Liu, Z.; Vaughan, M.; Powell, K.; Trepte, C. Caliop and aeronet aerosol optical depth comparisons: One size fits none. *J. Geophys. Res. Atmos.* **2013**, *118*, 4748–4766. [[CrossRef](#)]
74. Morcrette, J.-J.; Boucher, O.; Jones, L.; Salmond, D.; Bechtold, P.; Beljaars, A.; Benedetti, A.; Bonet, A.; Kaiser, J.; Razing, M.; et al. Aerosol analysis and forecast in the european centre for medium-range weather forecasts integrated forecast system: Forward modeling. *J. Geophys. Res. Atmos.* **2009**, *114*, doi:10.1029/2008JD011235. [[CrossRef](#)]
75. Benedetti, A.; Morcrette, J.-J.; Boucher, O.; Dethof, A.; Engelen, R.; Fisher, M.; Flentje, H.; Huneeus, N.; Jones, L.; Kaiser, J.; et al. Aerosol analysis and forecast in the european centre for medium-range weather forecasts integrated forecast system: 2. Data assimilation. *J. Geophys. Res. Atmos.* **2009**, *114*, doi:10.1029/2008JD011115. [[CrossRef](#)]
76. Eskes, H.; Huijnen, V.; Arola, A.; Benedictow, A.; Blechschmidt, A.; Botek, E.; Boucher, O.; Bouarar, I.; Chabrilat, S.; Cuevas, E.; et al. Validation of reactive gases and aerosols in the macc global analysis and forecast system. *Geosci. Model Dev.* **2015**, *8*, 3523. [[CrossRef](#)]
77. Reddy, M.S.; Boucher, O.; Bellouin, N.; Schulz, M.; Balkanski, Y.; Dufresne, J.-L.; Pham, M. Estimates of global multicomponent aerosol optical depth and direct radiative perturbation in the laboratoire de météorologie dynamique general circulation model. *J. Geophys. Res. Atmos.* **2005**, *110*, doi:10.1029/2004JD004757. [[CrossRef](#)]
78. Molod, A.; Takacs, L.; Suarez, M.; Bacmeister, J. Development of the geos-5 atmospheric general circulation model: Evolution from merra to merra2. *Geosci. Model Dev.* **2015**, *8*, 1339. [[CrossRef](#)]
79. Rienecker, M.; Suarez, J.; Todling, R.; Bacmeister, J.; Takacs, L.; Liu, H.; Gu, W.; Sienkiewicz, M.; Koster, R.; Gelaro, R.; et al. *The GEOS-5 Data Assimilation System- Documentation of Versions 5.0.1, 5.1.0, and 5.2.0*; Technical Report Series on Global Modeling and Data Assimilation; NASA Goddard Space Flight Center: Greenbelt, MD, USA, 2008; Volume 27.
80. Kleist, D.T.; Parrish, D.F.; Derber, J.C.; Treadon, R.; Wu, W.-S.; Lord, S. Introduction of the gsi into the ncep global data assimilation system. *Weather Forecast.* **2009**, *24*, 1691–1705. [[CrossRef](#)]
81. Wu, W.-S.; Purser, R.J.; Parrish, D.F. Three-dimensional variational analysis with spatially inhomogeneous covariances. *Mon. Weather Rev.* **2002**, *130*, 2905–2916. [[CrossRef](#)]
82. Randles, C.; da Silva, A.M.; Buchard, V.; Colarco, P.; Darmenov, A.; Govindaraju, R.; Smirnov, A.; Holben, B.; Ferrare, R.; Hair, J.; et al. The merra-2 aerosol reanalysis, 1980 onward. part i: System description and data assimilation evaluation. *J. Clim.* **2017**, *30*, 6823–6850. [[CrossRef](#)]
83. Randles, C.; da Silva, A.; Buchard, V.; Darmenov, A.; Colarco, P.; Aquila, V.; Bian, H.; Nowottnick, E.; Pan, X.; Smirnov, A.; et al. *The MERRA-2 Aerosol Assimilation*; NASA Technical Report Series on Global Modeling Data Assimilation; NASA Goddard Space Flight Center: Greenbelt, MD, USA, 2016; Volume 45.

84. McCarty, W.; Coy, L.; Gelaro, R.; Huang, A.; Merkova, D.; Smith, E.; Sienkiewicz, M.; Wargan, K. *Merra-2 input Observations: Summary and Assessment*; NASA Technical Report Series on Global Modeling and Data Assimilation; NASA Goddard Space Flight Center: Greenbelt, MD, USA, 2016.
85. Diner, D.J.; Abdou, W.A.; Bruegge, C.J.; Conel, J.E.; Crean, K.A.; Gaitley, B.J.; Helmlinger, M.C.; Kahn, R.A.; Martonchik, J.V.; Pilorz, S.H.; et al. MISR aerosol optical depth retrievals over southern Africa during the SAFARI-2000 dry season campaign. *Geophys. Res. Lett.* **2001**, *28*, 3127–3130. [[CrossRef](#)]
86. Qi, Y.; Ge, J.; Huang, J. Spatial and temporal distribution of MODIS and MISR aerosol optical depth over northern China and comparison with AERONET. *Chin. Sci. Bull.* **2013**, *58*, 2497–2506. [[CrossRef](#)]
87. Zeng, S.; Cornet, C.; Parol, F.; Riedi, J.; Thieuleux, F. A better understanding of cloud optical thickness derived from the passive sensors modis/aqua and polder/parasol in the a-train constellation. *Atmos. Chem. Phys.* **2012**, *12*, 11245–11259. [[CrossRef](#)]
88. Schutz, L. Sahara dust transport over the North Atlantic Ocean-Model calculations and measurements. In *Saharan Dust: Mobilization, Transport, Deposition*; Wiley: Chichester, UK, 1979; pp. 233–242.
89. Müller, D.; Weinzierl, B.; Petzold, A.; Kandler, K.; Ansmann, A.; Müller, T.; Tesche, M.; Freudenthaler, V.; Esselborn, M.; Heese, B.; et al. Mineral dust observed with AERONET Sun photometer, Raman lidar and in situ instruments during SAMUM 2006: Shape-independent particle properties. *J. Geophys. Res. Atmos.* **2010**, *115*. [[CrossRef](#)]
90. Reid, J.S.; Jonsson, H.H.; Maring, H.B.; Smirnov, A.; Savoie, D.L.; Cliff, S.S.; Reid, E.A.; Linvingston, J.M.; Meier, M.M.; Dubovik, O.; et al. Comparison of size and morphological measurements of coarse mode dust particles from Africa. *J. Geophys. Res. Atmos.* **2003**, *108*, doi:10.1029/2002JD002485. [[CrossRef](#)]
91. Toledano, C.; Wiegner, M.; Groß, S.; Freudenthaler, V.; Gasteiger, J.; Müller, D.; Schladitz, A.; Weinzierl, B.; Torres, B.; O’neill, O.O. Optical properties of aerosol mixtures derived from sun-sky radiometry during SAMUM-2. *Tellus B Chem. Phys. Meteorol.* **2011**, *63*, 635–648. [[CrossRef](#)]
92. Weinzierl, B.; Ansmann, A.; Prospero, J.; Althausen, D.; Benker, N.; Chouza, F.; Dollner, M.; Farrell, D.; Fomba, W.; Freudenthaler, V.; et al. The saharan aerosol long-range transport and aerosol–cloud-interaction experiment: Overview and selected highlights. *Bull. Am. Meteorol. Soc.* **2017**, *98*, 1427–1451. [[CrossRef](#)]
93. Diner, D.J.; Beckert, J.C.; Reilly, T.H.; Ackeman, T.; Bruegge, C.J.; Conel, J.E.; Davies, R.; Gerstl, S.A.W.; Gordon, H.R.; Kahn, R.A.; et al. Multi-angle imaging spectroradiometer (MISR): Instrument description and experiment overview. *IEEE Trans. Geosci. Remote Sens.* **1998**, *36*, 1500–1530. [[CrossRef](#)]
94. Lyapustin, A.; Wang, Y. *MAIAC Multi-Angle Implementation of Atmospheric Correction for MODIS*; Algorithm Theoretical Basis Document (ATBD, Version 1.0); NASA: Washington, DC, USA, 2008; Volume 127, pp. 385–393. [[CrossRef](#)]
95. Lange, C.B.; Romero, O.E.; Wefer, G.; Gabric, A.J. Offshore influence of coastal upwelling off mauritania, nw africa, as recorded by diatoms in sediment traps at 2195 m water depth. *Deep. Sea Res. Part Oceanogr. Res. Pap.* **1998**, *45*, 985–1013. [[CrossRef](#)]
96. Monahan, A.H. Empirical models of the probability distribution of sea surface wind speeds. *J. Clim.* **2007**, *20*, 5798–5814. [[CrossRef](#)]
97. Kahn, R.A.; Garay, M.J.; Nelson, D.L.; Yau, K.K.; Bull, M.A.; Gaitley, B.J.; Martonchik, J.V.; Levy, R.C. Satellite-derived aerosol optical depth over dark water from misr and modis: Comparisons with aeronet and implications for climatological studies. *J. Geophys. Res. Atmos.* **2007**, *112*, [[CrossRef](#)]
98. Goudie, A.S.; Middleton, N.J. The changing frequency of dust storms through time. *Clim. Chang.* **1992**, *20*, 197–225. [[CrossRef](#)]
99. N’Tchayi, G.M.; Bertrand, J.; Legrand, M.; Baudet, J. Temporal and spatial variations of the atmospheric dust loading throughout West Africa over the last thirty years. *Ann. Geophys.* **1994**, *12*, 265–273. [[CrossRef](#)]
100. Mahowald, N.M. Anthropocene changes in desert area: Sensitivity to climate model predictions. *Geophys. Res. Lett.* **2007**, *34*, doi:10.1029/2007GL030472. [[CrossRef](#)]
101. Andrea, M. Biomass burning: Its history, use and distribution and its impact on environmental quality and global change. In *Global Biomass Burning: Atmospheric, Climatic, and Biospheric Implications*; MIT Press: Cambridge, MA, USA, 1991; pp. 3–21.
102. Dubief, J. Review of the North African climate with particular emphasis on the production of eolian dust in the Sahel zone and in the Sahara. In *Saharan Dust: Mobilization, Transport, Deposition*; Morales, C., Ed.; Wiley & Sons: Hoboken, NJ, USA, 1979; pp. 27–48.

103. Huang, J.; Zhang, C.; Prospero, J.M. African dust outbreaks: A satellite perspective of temporal and spatial variability over the tropical atlantic ocean. *J. Geophys. Res. Atmos.* **2010**, *115*, doi:10.1029/2009JD012516. [[CrossRef](#)]
104. Schutz, L. Long range transport of desert dust with special emphasis on the Sahara. *Ann. N. Y. Acad. Sci.* **1980**, *338*, 515–532. [[CrossRef](#)]
105. Yu, H.; Chin, M.; Bian, H.; Yuan, T.; Prospero, J.M.; Omar, A.; Winker, L.R.D.; Yang, Y.; Zhang, Y.; Zhang, Y. Quantification of trans-Atlantic dust transport from seven-year (2007–2013) record of CALIPSO lidar measurements. *Remote Sens. Environ.* **2015**, *159*, 232–249. [[CrossRef](#)]
106. van der Does, M.; Korte, L.F.; Munday, C.I.; Brummer, G.-J.A.; Stuut, J.-B.W. Particle size traces modern saharan dust transport and deposition across the equatorial north atlantic. *Atmos. Chem. Phys.* **2016**, *16*, 13697. [[CrossRef](#)]
107. Velasco-Merino, C.; Mateos, D.; Toledano, C.; Prospero, J.M.; Molinie, J.; Euphrasie-Clotilde, L.; González, R.; Cachorro, V.E.; Calle, A.; de Frutos, A. Impact of long-range transport over the atlantic ocean on saharan dust optical and microphysical properties. *Atmos. Chem. Phys. Discuss.* **2018**. [[CrossRef](#)]
108. Yang, W.; Marshak, A.; Várnai, T.; Kalashnikova, O.V.; Kostinski, A.B. Calipso observations of transatlantic dust: Vertical stratification and effect of clouds. *Atmos. Chem. Phys.* **2012**, *12*, 11339–11354. [[CrossRef](#)]
109. Bellouin, N.; Quaas, J.; Morcrette, J.-J.; Boucher, O. Estimates of aerosol radiative forcing from the macc re-analysis. *Atmos. Chem. Phys.* **2013**, *13*, 2045–2062. [[CrossRef](#)]
110. Adams, A.M.; Prospero, J.M.; Zhang, C. Calipso-derived three-dimensional structure of aerosol over the atlantic basin and adjacent continents. *J. Clim.* **2012**, *25*, 6862–6879 [[CrossRef](#)]
111. Nicholson, S.E. The nature of rainfall variability over africa on time scales of decades to millenia. *Glob. Planet. Chang.* **2000**, *26*, 137–158. [[CrossRef](#)]
112. Peyridieu, S.; Chédin, A.; Capelle, V.; Tsamalis, C.; Pierangelo, C.; Armante, R.; Crevoisier, C.; Crépeau, L.; Siméon, M.; Ducos, F.; et al. Characterisation of dust aerosols in the infrared from iasi and comparison with parasol, modis, misr, caliop, and aernet observations. *Atmos. Chem. Phys.* **2013**, *13*, 6065–6082. [[CrossRef](#)]
113. Denjean, C.; Formenti, P.; Desboeufs, K.; Chevaillier, S.; Triquet, S.; Maillé, M.; Cazaunau, M.; Laurent, B.; Mayol-Bracero, O.L.; Vallejo, P.; et al. Size distribution and optical properties of african mineral dust after intercontinental transport. *J. Geophys. Res. Atmos.* **2016**, *121*, 7117–7138. [[CrossRef](#)]
114. Ridley, D.; Heald, C.; Ford, B. North african dust export and deposition: A satellite and model perspective. *J. Geophys. Res. Atmos.* **2012**, *117*, doi:10.1029/2011JD016794. [[CrossRef](#)]
115. Kim, D.; Chin, M.; Yu, H.; Diehl, T.; Tan, Q.; Kahn, R.A.; Tsigaridis, K.; Bauer, S.E.; Takemura, T.; Pozzoli, L.; et al. Sources, sinks, and transatlantic transport of north african dust aerosol: A multimodel analysis and comparison with remote sensing data. *J. Geophys. Res. Atmos.* **2014**, *119*, 6259–6277. [[CrossRef](#)]
116. Guo, Y.; Tian, B.; Kahn, R.A.; Kalashnikova, O.; Wong, S.; Waliser, D.E. Tropical Atlantic dust and smoke aerosol variations related to the Madden-Julian Oscillation in MODIS and MISR observations. *J. Geophys. Res. Atmos.* **2013**, *118*, 4947–4963. [[CrossRef](#)]
117. Kalu, A. The african dust plume: Its characteristics and propagation across west africa in winter. *Scope* **1979**, *14*, 95–118.
118. Chiapello, I.; Bergametti, G.; Gomes, L.; Chatenet, B.; Dulac, F.; Pimenta, J.; Soares, E.S. An additional low layer transport of Sahelian and Saharan dust over the north-eastern tropical Atlantic. *Geophys. Res. Lett.* **1995**, *22*, 3191–3194. [[CrossRef](#)]
119. Ansmann, A.; Rittmeister, F.; Engelmann, R.; Basart, S.; Jorba, O.; Spyrou, C.; Remy, S.; Skupin, A.; Baars, H.; Seifert, P.; et al. Profiling of saharan dust from the caribbean to western Africa—Part 2: Shipborne lidar measurements versus forecasts. *Atmos. Chem. Phys.* **2017**, *17*, 14987–15006. [[CrossRef](#)]
120. Kok, J.F. A scaling theory for the size distribution of emitted dust aerosols suggests climate models underestimate the size of the global dust cycle. *Proc. Natl. Acad. Sci. USA* **2011**, *108*, 1016–1021. [[CrossRef](#)]

